A Theory of Crack Growth in Viscoelastic Media

Texas A and M University

prepared for

Office of Naval Research

MARCH 1973

Mechanics and Materials Research Center
TEXAS A&M UNIVERSITY
College Station, Texas

A THEORY OF CRACK GROWTH IN VISCOELASTIC MEDIA

R. A. SCHAPERY

Office of Naval Research
Department of the Navy
Contract No. N00014-68-A-0308-0003
Task Order NR 064-520
Technical Report No. 2

MM 2764-73-1

March 1973

Unclassified

Security Classification

DOCUMENT CONTROL DATA - R & D

(Security classification of title, body of abstract and indexing annotation must be entered when the overall report is classified)

1. ORIGINATING ACTIVITY (Corporate author) Texas A&M University Texas Engineering Experiment Station	2a. REPORT SECURITY CLASSIFICATION Unclassified 2b. GROUP N/A

3. REPORT TITLE

A THEORY OF CRACK GROWTH IN VISCOELASTIC MEDIA

4. DESCRIPTIVE NOTES (Type of report and inclusive dates)

Technical Report

5. AUTHOR(S) (First name, middle initial, last name)

R. A. Schapery

6. REPORT DATE	7a. TOTAL NO. OF PAGES	7b. NO. OF REFS
March, 1973		

8a. CONTRACT OR GRANT NO.	9a. ORIGINATOR'S REPORT NUMBER(S)
N00014-68-A-0308-0003 b. PROJECT NO. NR 064-520 c. d.	MM2764-73-1 9b. OTHER REPORT NO(S) (Any other numbers that may be assigned this report)

10. DISTRIBUTION STATEMENT

Approved for public release; Distribution unlimited

11. SUPPLEMENTARY NOTES	12. SPONSORING MILITARY ACTIVITY
	Department of the Navy Office of Naval Research Arlington, Virginia 22217

13. ABSTRACT

A theory is developed for predicting the time-dependent size and shape of cracks in linearly viscoelastic, isotropic media, and its validity is demonstrated by applying the theory to crack growth and failure of unfilled and particulate-filled polymers. Starting with a bounded solution for the stress distribution near a crack tip in an elastic body and the extended correspondence principle for viscoelastic media with moving boundaries, a simple equation is derived for predicting instantaneous crack tip velocity in terms of the opening-mode stress intensity factor; although the undamaged portion of the continuum is assumed linear, no significant restrictions are placed on the nature of the disintegrating material near the crack tip and, therefore, this material may be highly nonlinear, rate-dependent, and even discontinuous. A further analysis is made to predict the time at which a crack starts to grow, and then some explicit solutions are given for this so-called fracture initiation time, the time-dependent crack growth, and the time at which gross failure occurs under time-varying applied forces and environmental parameters. Following a derivation of the linear cumulative damage rule, an examination of its theoretical range of validity, and a discussion of the experimental determination of fracture properties, the theory is applied to monolithic and composite materials under constant and varying loads. Some concluding remarks deal with extensions of the theory to include finite strain effects, crack growth in the two shearing modes and in combined opening and shearing modes, and adhesive fracture.

DD FORM 1 NOV 65 1473 (PAGE 1)

S/N 0101-807-6801

Unclassified

Security Classification

14 KEY WORDS	LINK A		LINK B		LINK C	
	ROLE	WT	ROLE	WT	ROLE	WT
Fracture Mechanics						
Viscoelasticity						
Polymers						
Crack Propagation						
Fatigue						

Mechanics and Materials Research Center

Texas Engineering Experiment Station

TEXAS A&M UNIVERSITY

College Station, Texas 77843

A THEORY OF CRACK GROWTH IN VISCOELASTIC MEDIA

by

R. A. Schapery

Civil and Aerospace Engineering Departments

This work was sponsored by the

Office of Naval Research

Department of the Navy

Contract No. N00014-68-A-0308-0003

Task Order NR 064-520

Technical Report No. 2

MM2764-73-1

March 1973

ic

ABSTRACT

A theory is developed for predicting the time-dependent size and shape of cracks in linearly viscoelastic, isotropic media, and its validity is demonstrated by applying the theory to crack growth and failure of unfilled and particulate-filled polymers. Starting with a bounded solution for the stress distribution near a crack tip in an elastic body and the extended correspondence principle for viscoelastic media with moving boundaries, a simple equation is derived for predicting instantaneous crack tip velocity in terms of the opening-mode stress intensity factor; although the undamaged portion of the continuum is assumed linear, no significant restrictions are placed on the nature of the disintegrating material near the crack tip and, therefore, this material may be highly nonlinear, rate-dependent, and even discontinuous. A further analysis is made to predict the time at which a crack starts to grow, and then some explicit solutions are given for this so-called fracture initiation time, the time-dependent crack growth, and the time at which gross failure occurs under time-varying applied forces and environmental parameters. Following a derivation of the linear cumulative damage rule, an examination of its theoretical range of validity, and a discussion of the experimental determination of fracture properties, the theory is applied to monolithic and composite materials under constant and varying loads. Some concluding remarks deal with extensions of the theory to include finite strain effects, crack growth in the two shearing modes and in combined opening and shearing modes, and adhesive fracture.

TABLE OF CONTENTS

1. Introduction

Prediction of the mechanical response and service life of viscoelastic structures is very much dependent on one's ability to predict the time-dependent growth of flaws or cracks. This growth affects not only the time of gross failure, but, in the case of composite materials, may also have an appreciable influence on the effective mechanical behavior long before structural failure occurs [1].

In this paper we focus our attention on the movement of a single crack tip or front, and establish and apply relatively simple equations for predicting the time at which motion initiates (the "fracture initiation time") as well as the instantaneous tip velocity, both in terms of the opening-mode stress intensity factor. Interactions between two or more cracks and the influence of boundaries and obstacles are implicitly taken into account through this stress intensity factor. For reasons of mathematical simplicity, the material in a small neighborhood surrounding the crack tip is divided into two regions: (i) a failure zone where disintegration and eventual failure occur, and (ii) a linearly viscoelastic, macroscopically homogeneous and isotropic inertialess continuum. This idealization and some later mathematical approximations are motivated by certain characteristics of viscoelastic behavior which are common to many different polymeric materials. However, this motivation does not mean the theory is limited to polymers; indeed,

it contains as a special case the classical theory of fracture for elastic and elastic-perfectly plastic media when the plastic zone size is small relative to crack length.

We shall not attempt to review or even list the many experimental and theoretical papers which now exist on the subject of crack growth in viscoelastic materials. Instead, the reader is referred to the excellent review article by Knauss [2], which covers molecular processes, stress analysis, crack propagation concepts, heat evolution effects (which we neglect in this paper), and environmental influences. Primarily only those studies which are closely related to the present one are discussed here.

There already exist some theories for predicting fracture initiation time and crack growth in the opening mode in linear viscoelastic media. Williams [3] used the idealized geometry of a disintegrating hollow sphere to establish the essential dependence of fracture initiation time and initial crack velocity on external loading history. Wnuk and Knauss [4] derived an equation for fracture initiation time of a penny-shaped crack in a viscoelastic-perfectly plastic solid, and gave solutions for a Maxwell material and general linear viscoelastic solid having a time-dependent and time-independent yield stress, respectively. In order to predict crack growth following initiation, Knauss and co-workers [5-7] modeled the disintegrating material near the crack tip by assuming bi-singular stress and displacement distributions and using a rather idealized mechanism for calculating the transfer

of energy from the linear viscoelastic continuum to the intermolecular or interatomic bonds. Kostrov and Nikitin [8] derived an equation governing crack growth in a linearly viscoelastic-perfectly plastic solid, studied its consequences for the Griffith problem of a crack in a large sheet under constant stress, and gave an explicit solution for a Maxwell material.

One distinguishing feature of existing theories on crack growth is that the failing material near the crack tip is replaced by a very idealized model. Another feature is that solutions for the time-dependent crack size are given numerically or, if analytical, are for severely idealized media (e.g., a Maxwell material). The present study was undertaken primarily to remove these two limitations, and is accomplished by introducing one new assumption: the second derivative of the logarithm of creep compliance with respect to logarithm of time is small for the linear viscoelastic continuum. To the writer's knowledge, all polymeric structural materials of technological interest satisfy this assumption over all or most of the time range of variation of the creep compliance. Even if there are intervals over which the curvature is not small, the theory is valid whenever the effective time parameter (Eq. (92a)) is outside of these intervals.

The fact that the failure process at the crack tip is quite arbitrary in the present theory implies the theory should be valid for many different materials, including polymers exhibiting the crazing phenomenon [9] and filled polymers. This point is supported

in Section 4 by successfully predicting crack growth and failure of an unfilled rubber (Solithane) and two particulate composites (solid propellant and asphaltic concrete) under constant and varying loads. Moreover, because of the simplicity and generality of the theory, we believe it will be useful for a variety of applications, such as the prediction of effective viscoelastic properties of composite media having "microstructural damage" [1], fatigue crack growth, and the statistical distribution of failure times of monolithic and composite materials in terms of fundamental property and flaw size distributions [10].

We now turn to a study of the elastic and viscoelastic distributions of stresses and displacement near the crack tip. The nature of these distributions is examined in some detail in order to provide a basis for making certain later approximations.

2. Stress and Displacement Distributions Near the Crack Tip

The problem considered in this Section is that of predicting stresses and displacements in the vicinity of a crack tip in which, for simplicity, the relative displacement between the crack surfaces is taken normal to them; i.e., the so-called "opening mode" is assumed.

A fixed (x,y) coordinate system and the idealized tip geometry are shown in Fig. 1; $y = 0$ will always correspond to the plane of the crack, while the y-axis is placed at any convenient location and embedded in the continuum. In the unstrained state the crack surfaces near the tip are assumed to be planar and to coincide with the x-z plane, where z is perpendicular to the plane of the page. The actual crack tip is a straight or curved line in space whose intersection with the x-y plane (the plane of the page) is defined by the point P $(x = a, y = 0)$; it is assumed that the tip is essentially straight in the neighborhood of P and perpendicular to the x-y plane. We should add "neighborhood of the point P" refers simply to the material contained in a spherical volume centered at P and having dimensions on the order of the failure zone width, α; P is taken to be a generic location along the crack tip and, therefore, the term "neighborhood (or vicinity) of the crack tip" will be used to mean the same thing as "neighborhood of P" throughout this paper.

The crack tip may be quite general in shape as far as our analysis is concerned. For example, it may be a closed curve or begin and end on bounding surfaces of the continuum; of course, the first case

corresponds to an "internal" crack, while the crack tip in the second case defines "through" and "surface" cracks.

We assume the material outside of the failure zone shown in Fig. 1 is linearly viscoelastic. However, in general, the material in the zone may be highly nonlinear and viscoelastic; further, it need not be a continuum in that it could consist of very fine strands or any other disintegrating material which is representative of the complex structure near a crack tip, or the failure zone could be simply the region in which significant attractive interatomic forces act between atoms in adjacent crack surfaces. In practice, the boundary between the undamaged continuum and the material in the failure zone will be rather diffuse, and there will be a layer of damaged material which extends into the continuum along $x < a_a$ as well as around the failure zone; we assume this layer is small enough that its effect on the prediction of the displacement v in the neighborhood of the tip is negligible.

The location $x = a_a$ defines the apparent crack tip, which is often referred to in the literature as the crack tip. However, in contrast, throughout this paper crack tip will mean the tip at $x = a$.

The reaction of the failure zone on the surrounding continuum is represented by a tensile stress distribution, σ_f, as shown in Fig. 2, while σ_y denotes the tensile stress acting within the linearly viscoelastic material along the crack's prolongation. External loads applied to the continuum are assumed to act symmetrically with respect to the crack, so that shearing stresses along $x > a$ are zero

and a pure crack opening mode results.

However, in reality, shearing stresses act along the continuum within the failure zone. This may be seen by referring to Fig. 3, which shows the forces acting on the material in this zone; the tip has been magnified to bring out the tip thickness, d_i, which is taken to be a characteristic dimension defining an interatomic distance before failure in the case of a monolithic material, or an interparticle distance in the case of a particulate composite. As will be seen later, the stress σ_x acting along $x > a$ is equal to σ_y and, therefore, $F_i \simeq \sigma_y d_i$ (per unit length of crack tip). Thus, a rough estimate of the average shearing stress, τ_f, is

$$\tau_f \equiv \frac{F_x}{\alpha} \simeq \frac{\sigma_y}{2} \frac{d_i}{\alpha} \quad . \tag{1}$$

Consequently, as long as $\alpha >> d_i$, it is reasonable to neglect the effect of τ_f, relative to that of σ_f, on the surrounding linear viscoelastic material; this condition is consistent with that needed to be able to apply continuum mechanics in the first place to predicting the response of (assumed) homogeneous material close to the failure zone.

Although Figs.1 and 2 show the crack surface for $x < a_a$ as being stress-free, the theory allows for forces to act directly on the crack surface, as long as they are not applied in the neighborhood of the tip. If external forces are close to the tip, the theory will be at least approximately valid when they are small relative to the resultant failure force. (It is of interest to point out that an

important geological problem in which there is direct pressure on crack faces, viz., fracture of oil-bearing rock strata, satisfies this condition; there is always an unwetted portion near the crack tips [11].)

Finally, it is assumed that the neighborhood of the point P in Fig. 1 is in a state of plane strain. This condition is (approximately) satisfied if (i) the distance between P and bounding surfaces of the continuum and other cracks is large compared to α; (ii) the radius of curvature of the crack tip at P is much larger than α; and (iii) the value of σ_z outside the neighborhood of P is small relative to σ_y inside the neighborhood. Of course, if one is interested in the problem of "through crack" in a thin sheet in which α is large compared to sheet thickness, the plane strain results are converted to this plane stress situation by means of a simple change in the solution; i.e., ν^2 in Eq. (7) is dropped.

Linear Elastic Analysis

Stress and displacement distributions along $y = 0$ in the neighborhood of the crack tip are recorded here for later extension to viscoelasticity. We first consider stresses σ_x^o and σ_y^o, and displacement v^o (say) due to loads acting in and on a linear elastic continuum having a crack tip at $x = a$ and with $\sigma_f \equiv 0$. Based on the results given by Williams [12], we may write*

$$\sigma_x^o = \frac{N_o}{\sqrt{\xi_1}} H(\xi_1)[1 + O(\xi_1/\beta)] \tag{2}$$

*A term of order μ is written as $O(\mu)$ for which, by definition, $\lim_{\mu \to 0} [O(\mu)/\mu]$ = finite, non-zero quantity.

$$\sigma_y^o = \frac{N_o}{\sqrt{\xi_1}} H(\xi_1)[1 + O(\xi_1/\beta)] \tag{3}$$

while the displacement of the top crack face is (for plane strain)

$$v^o = C_e N_o \sqrt{\xi} H(\xi)[1 + O(\xi/\beta)] \tag{4}$$

where (see Fig. 2)

$$\xi_1 \equiv x - a \quad , \quad \xi \equiv a - x \quad . \tag{5}$$

Also, $H(\rho)$ is the unit-step function:

$$H(\rho) \equiv \begin{cases} 0 \ , \ \rho < 0 \\ 1 \ , \ \rho > 0 \end{cases} \tag{6}$$

and

$$C_e \equiv \frac{4(1 - \nu^2)}{E} \tag{7}$$

where E is Young's modulus and ν is Poisson's ratio. The coefficient N_o is called the stress intensity factor by Barenblatt [11]; this factor is simply related to another commonly used symbol, K_I, for the opening-mode stress intensity factor

$$K_I \equiv \sqrt{2\pi} N_o \quad . \tag{8}$$

In general, N_o is a functior of Young's modulus and Poisson's ratio as well as parameters which define the geometry of the continuum (e.g., crack length and location and overall dimensions of the body) and is a linear function of the applied loads and displacements.

The quantity β represents the distance between the point P (Fig. 1) and the closest geometric feature (e.g., free surface or opposite crack tip) or nearest point of load application, depending on which is smallest. By restricting ξ and ξ_1 to the neighborhood of P and assuming

$$\alpha/\beta << 1 \tag{9}$$

the terms of order ξ_1/β and ξ/β can be neglected since

$$O(\frac{\xi_1}{\beta}) = O(\frac{\alpha}{\beta}\frac{\xi_1}{\alpha}) \quad ; \quad O(\frac{\xi}{\beta}) = O(\frac{\alpha}{\beta}\frac{\xi_1}{\alpha}) \ . \tag{10}$$

Hence, close to the crack tip

$$\sigma_x^o = \sigma_y^o = \frac{N_o}{\sqrt{\xi_1}} H(\xi_1) \tag{11}$$

$$v^o = C_e N_o \sqrt{\xi}\, H(\xi) \ . \tag{12}$$

Stresses and displacement in the linear solid due to the failure stress, σ_f, acting <u>alone</u> are denoted by σ_x^f, σ_y^f, and v^f. From Barenblatt [11], for $\xi_1 > 0$,

$$\sigma_x^f = \sigma_y^f = -\frac{1}{\pi\sqrt{\xi_1}} \int_o^\alpha \frac{\sqrt{\xi}\ \sigma_f(\xi)\ d\xi}{\xi + \xi_1} \tag{13}$$

and the displacement of the top crack face is

$$v^f = -\frac{C_e}{2\pi} H(\xi) \mathcal{R}\left\{ \int_0^\alpha \sigma_f(\xi') \ln\left[\frac{\sqrt{\xi'} + \sqrt{\xi}}{\sqrt{\xi'} - \sqrt{\xi}}\right] d\xi' \right\} \qquad (14a)$$

where $\mathcal{R}$ denotes "real part of"; inasmuch as $\ln(-1) = i\,\pi(2k + 1)$, $k = 0,1,2,\ldots$, the last equation can be written in real notation as

$$v^f = -\frac{C_e}{2\pi} H(\xi) \int_0^\alpha \sigma_f(\xi') \ln\left|\frac{\sqrt{\xi'} + \sqrt{\xi}}{\sqrt{\xi'} - \sqrt{\xi}}\right| d\xi' \quad . \qquad (14b)$$

On physical grounds it is assumed that σ_f is everywhere finite, which assures uniform convergence of the above integrals, Eqs. (13) and (14), for $\xi_1 \geq 0$ and $\xi \geq 0$. Although the failure stress is <u>not</u> restricted to being continuous for all ξ, we do make the physically plausible assumption that it is continuous to the left at $\xi = 0$; viz.

$$\lim_{\xi \to 0^+} \sigma_f(\xi) = \sigma_f(0) \quad . \qquad (15)$$

As will be seen later, existence of the limit in Eq. (15) together with the assumption that the stresses in the linear continuum are finite establishes continuity of the tensile stress in the y-direction at $y = \xi = 0$; even if Eq. (15) is not met, it can be shown that the stress immediately to the right of the tip, $\sigma_y(0^+)$, still will be equal to the failure stress on the left side of the tip, $\sigma_f(0^+)$.

Of particular interest to us is the behavior of stresses, Eq. (13), and displacement, Eq. (14), close to the crack tip; viz., $\xi_1/\alpha \ll 1$ and

$\xi/\alpha \ll 1$. The stresses become [11]

$$\sigma_x^f = \sigma_y^f = -\frac{1}{\pi\sqrt{\xi_1}} \int_0^\alpha \frac{\sigma_f(\xi)}{\sqrt{\xi}}\, d\xi + \sigma_f(0) + 0(\xi_1^{1/2}) \quad . \tag{16}$$

Although not stated in [11], the order of the remainder term in Eq. (16), as well as the remainder shown later in displacement Eq. (25), is correct only if σ_f satisfies the following condition:

$$\lim_{\xi \to 0^+} \{[\sigma_f(\xi) - \sigma_f(0)]/\xi^{1/2}\} = 0 \tag{17}$$

which will be established and discussed later in this subsection. The resultant stresses in the linear continuum due the combined action of the failure stress distribution and the externally and internally applied loads are obtained by adding Eq. (11) and (16). These stresses will be finite at the tip if and only if

$$N_o = \frac{1}{\pi} \int_0^\alpha \frac{\sigma_f(\xi)\, d\xi}{\sqrt{\xi}} \tag{18}$$

which is Barenblatt's result [11]. The resultant stresses in the vicinity of tne crack tip become for $\xi_1 \geq 0$:

$$\sigma_x = \sigma_y = \sigma_f(0) + 0(\xi_1^{1/2}) \tag{19a}$$

A more complete representation is obtained by adding Eqs. (11) and (13) and then using Eq. (18):

$$\sigma_x = \sigma_y = \frac{1}{\pi}\sqrt{\xi_1}\int_0^{\alpha}\frac{\sigma_f(\xi)}{\sqrt{\xi}\,(\xi+\xi_1)}\,d\xi \quad . \tag{19b}$$

Equation (19a) together with Eq. (15) implies the normal stress in the y-direction is continuous at $\xi_1 = 0$. For later convenience, we rewrite Eq. (18) in terms of a normalized coordinate,

$$\eta \equiv \xi/\alpha \tag{20}$$

and normalized failure stress distribution,

$$f \equiv \sigma_f/\sigma_m \tag{21}$$

where σ_m is the maximum of $\sigma_f(\xi)$ with respect to ξ; at this time there is no need to assume that $\sigma_f(0)$ is this maximum value. Equation (18) now becomes

$$N_o = \frac{\sqrt{\alpha}\,\sigma_m}{\pi} I_1 \tag{22}$$

in which I_1 is the dimensionless integral,

$$I_1 \equiv \int_0^1 \frac{f(\alpha\eta)}{\sqrt{\eta}}\,d\eta \quad . \tag{23}$$

One further change of integration variable to η', where $\eta' \equiv 2\sqrt{\eta}$, yields

$$I_1 = \int_0^2 f\,d\eta' \quad . \tag{24a}$$

Since $f \leq 1$,

$$I_1 \leq 2 \tag{24b}$$

which will prove useful in later considerations in order to establish a lower bound on the maximum strength, σ_m, from experimental data.

The normalized form, Eq. (22), is a very important result. It will enable us to calculate the length of the failure zone, α, as a function of time and loading.

The displacement of the top crack face near the tip due to σ_f acting alone, as given by Barenblatt [11], is

$$v^f = -\frac{C_e}{\pi}\sqrt{\xi}\,H(\xi)\int_0^\alpha \frac{\sigma_f(\xi')d\xi'}{\sqrt{\xi'}} + \Delta v^f\,H(\xi) \tag{25}$$

where $\Delta v^f = O(\xi^{3/2})$. In order to predict time-dependent crack growth in viscoelastic materials we need more explicit representations of Δv^f; for one purpose it will be necessary to evaluate the coefficient of $\xi^{3/2}$ and establish the order of the remaining terms. This will be accomplished by first equating Eqs. (14b) and (25), which yields

$$\Delta v^f = \frac{C_e}{2\pi}\int_0^\alpha \sigma_f(\xi')\left\{2\left(\frac{\xi}{\xi'}\right)^{1/2} - \ln\left|\frac{\sqrt{\xi'}+\sqrt{\xi}}{\sqrt{\xi'}-\sqrt{\xi}}\right|\right\}d\xi' \quad . \tag{26}$$

It is important to observe that the resultant displacement, $v = v^o + v^f$, due to applied loads and to σ_f is simply related to Δv^f;

viz.,

$$v = \Delta v^f \, H(\xi) \tag{27}$$

which follows from Eqs. (12), (14b) and (18).

Determination of the behavior of Δv^f from Eq. (26) requires that we express σ_f in the form

$$\sigma_f(\xi) = \sigma_f(0) + \Delta\sigma_f(\xi) \quad . \tag{28}$$

In view of Eq. (15),

$$\lim_{\xi \to 0^+} \Delta\sigma_f(\xi) = 0 \quad . \tag{29}$$

Upon substituting Eq. (28) into Eq. (26) and evaluating the integral containing $\sigma_f(0)$ there results

$$\Delta v^f = \frac{2C_e}{3\pi} \frac{\sigma_f(0)}{\sqrt{\alpha}} [\xi^{3/2} + O(\xi^{5/2})] + \Delta I \tag{30}$$

where

$$\Delta I \equiv \frac{C_e}{2\pi} \int_0^\alpha \Delta\sigma_f(\xi') \left\{ 2\left(\frac{\xi}{\xi'}\right)^{1/2} - \ln\left| \frac{1 + \sqrt{\xi/\xi'}}{1 - \sqrt{\xi/\xi'}} \right| \right\} d\xi' \quad . \tag{31}$$

The term in curly brackets for $0 < \xi/\xi' \ll 1$ is approximately

$$\left\{ 2\left(\frac{\xi}{\xi'}\right)^{1/2} - \ln\left| \frac{1 + \sqrt{\xi/\xi'}}{1 - \sqrt{\xi/\xi'}} \right| \right\} \simeq -\frac{2}{3}\left(\frac{\xi}{\xi'}\right)^{3/2} - \frac{2}{5}\left(\frac{\xi}{\xi'}\right)^{5/2} \tag{32}$$

Without any approximation, Eq. (31) is now written as

$$\Delta I = -\frac{C_e}{3\pi}\,\zeta^{3/2}\int_0^{\alpha}\frac{\Delta\sigma_f(\xi')}{(\xi')^{3/2}}\,d\xi'$$

$$+\frac{C_e}{2\pi}\int_0^{\alpha}\Delta\sigma_f(\xi')\left\{2\left(\frac{\xi}{\xi'}\right)^{1/2}-\ln\left|\frac{1+\sqrt{\xi/\xi'}}{1-\sqrt{\xi/\xi'}}\right|\right.$$

$$\left.+\frac{2}{3}\left(\frac{\xi}{\xi'}\right)^{3/2}\right\}d\xi' \qquad (33)$$

If Eq. (17) is satisfied the first integral in Eq. (33) obviously converges; also, the second integral is easily shown to be convergent. This condition means, of course, that $\Delta\sigma_f$ must approach zero faster than $\xi^{1/2}$ as $\xi \to 0$. If this approach to zero is faster than $\xi^{3/2}$; viz.,

$$\lim_{\xi \to 0^+}\left[\Delta\sigma_f(\xi)/\xi^{3/2}\right] = 0 \qquad (34)$$

then it follows from Eqs. (32) and (33) that the second integral in Eq. (33) is of order $\xi^{5/2}$ or higher. In contrast, if Eq. (17) is satisfied, but not Eq. (34), then the order of the second integral in Eq. (33) is found to be between $\xi^{3/2}$ and $\xi^{5/2}$. Moreover, it is shown in Appendix A that if Eq. (17) is <u>not</u> met, the order of ΔI, Eq. (31), is between ξ and $\xi^{3/2}$.

Considering the complexity of the failure process at the crack tip, and the absence of information on the variation of $\sigma_f(\xi)$ for most materials [2], it will be assumed throughout the remainder of this paper that Eq. (17) holds, unless stated otherwise. Note that

if σ_f is constant (e.g., when the failure zone is actually the zone of yielding in a metal having zero strain hardening) not only will Eq. (34) be satisfied but additionally $\Delta I = 0$.

Let us now integrate the first integral in Eq. (33) by parts, use definition Eq. (28) for $\Delta\sigma_f$, replace the second integral by an order statement, and then substitute the result into Eq. (30); thus,

$$\Delta v^f = \frac{2C_e}{3\pi}\left[\frac{\sigma_f(\alpha^-)}{\sqrt{\alpha}} - \int_0^{\alpha^-}\frac{d\sigma_f}{d\xi'}\frac{d\xi'}{\sqrt{\xi'}}\right]\xi^{3/2} + O(\xi^{3/2+p}) \qquad (35)$$

where $0 < p \leq 1$, and $\sigma_f(\alpha^-)$ is the failure stress for ξ just to the right of α; of course, if σ_f is continuous at $\xi = \alpha$ there is no need to distinguish between $\xi = \alpha^-$ and $\xi = \alpha$. Equation (35) can be written more compactly in the form

$$\Delta v^f = -\frac{2C_e}{3\pi}\int_0^{\alpha^+}\frac{d\sigma_f}{d\xi'}\frac{d\xi'}{\sqrt{\xi'}}\,\xi^{3/2} + O(\xi^{3/2+p}) \quad . \qquad (36)$$

It is easily verified that Eq. (36) is equivalent to Eq. (35); when σ_f is discontinuous at $\xi = \alpha$ we may interpret $d\sigma_f/d\xi'$ by means of a Dirac delta function or, more directly, by using the relation

$$\int_0^{\alpha^+}\frac{d\sigma_f}{d\xi'}\frac{d\xi'}{\sqrt{\xi'}} = \int_0^{\alpha^-}\frac{d\sigma_f}{d\xi'}\frac{d\xi'}{\sqrt{\xi'}} + \int_{\alpha^-}^{\alpha^+}\frac{d\sigma_f}{d\xi'}\frac{d\xi'}{\sqrt{\xi'}}$$

$$= \int_0^{\alpha^-}\frac{d\sigma_f}{d\xi'}\frac{d\xi'}{\sqrt{\xi'}} + \frac{1}{\sqrt{\alpha}}\left[\cancel{\sigma_f}^{\,0}(\alpha^+) - \sigma_f(\alpha^-)\right] \quad . \qquad (37)$$

The total vertical displacement of the upper crack face due to external and internal loading and to the failure stresses is given by Eq. (27). After writing the integral in Eq. (36) in terms of the normalized variables, Eqs. (20) and (21), there results

$$v = -\frac{2C_e}{3\pi}\frac{\sigma_m}{\sqrt{\alpha}} I_2 \xi^{3/2} H(\xi) + O(\xi^{3/2 + p})\, H(\xi) \tag{38}$$

where $0 < p \leq 1$ and

$$I_2 \equiv \int_0^1 \frac{df}{d\eta}\frac{d\eta}{\sqrt{\eta}} \quad . \tag{39}$$

The upper limit in Eq. (39) is to be interpreted as 1^+ when f is discontinuous at $\eta = 1$; for example, if σ_f (and therefore f) is constant over $0 \leq \eta < 1$,

$$I_2 = -1 \quad . \tag{40}$$

Also, $p = 1$ for this case since $\Delta I = 0$.

The fact that $v = O(\xi^{3/2})$ according to Eq. (38), the cross-section of the crack near its tip (see Fig. 1) is cusp-shaped. This observation was made by Barenblatt [11]. However, as we have shown, this shape is predicted because Eq. (17) is assumed to be satisfied. On the other hand when this limit condition is <u>not</u> met, a study of ΔI, Eq. (31), in Appendix A reveals that the cross-section could approach a straight-sided wedge.

Finally, we should point out that the order of the stresses near the tip can be established in a manner that is entirely analogous to

the above one for displacement by starting with Eq. (19b); it is found, for example, that the remainder term in Eq. (19a) is indeed of order $\xi_1^{1/2}$ (or higher order when I_2, Eq. (39), vanishes) if Eq. (17) is obeyed. That the order of this term could range between ξ^0 and $\xi^{1/2}$ when this limit condition does not hold is shown in Appendix A. The order of the stresses, however, does not have a direct bearing on the subsequent viscoelastic analysis.

Linear Viscoelastic Analysis

With stationary cracks the elastic stress and displacement distributions given in the previous subsection can be easily generalized to viscoelastic solutions by means of the classical correspondence principle plus Laplace transform inversion [13].

Under somewhat restrictive conditions, the extended correspondence principle established by Graham [14] can be used with moving cracks. The specific restrictions as they apply to the problem at hand are (a) the crack cannot decrease in size ($da/dt \geq 0$); (b) the elastic stress normal to the surface of crack prolongation (σ_y) must be independent of E and ν; and (c) any dependence of the elastic displacement v along the crack face on E and ν must be in the form of a separate factor (i.e., $v = \text{fntn}(E,\nu) \cdot \text{fntn}(\xi)$). According to the theory in [14], the above restrictions apply to the entire crack and its extension up to the maximum time of interest, and not just the neighborhood of the instantaneous tip.

With reference to restriction (b), we note that as long as all

boundary conditions are on stress, dimensional analysis implies the internal stresses will be independent of Young's modulus, E; they may, in general, depend on Poisson's ratio, ν. Even this dependence on ν disappears in many two- and three-dimensional problems. Indeed, there are two important classes of plane stress and plane strain problems for which the in-plane stresses will always be independent of ν [15]: (i) simply-connected bodies and (ii) multiply-connected bodies for which the resultant force on each boundary vanishes. It should be added that if the viscoelastic material of interest has a constant Poisson's ratio (which is at least approximately true in many situations involving polymeric materials [1]), then dependence of the elastic solution on Poisson's ratio does not invalidate the extended correspondence principle; this last point is easily verified by examining Graham's theory [14]. As one further observation, we note that if some or all boundary conditions are on displacement, the problem often can be recast in terms of applied forces; one simply calculates the resultant forces needed to maintain the specified displacements, and then views these forces as being specified quantities. It will be assumed that such a recasting has been accomplished, when appropriate, in all of the following analyses; see, e.g., Eqs. (128) and (129).

Under the conditions for which the extended correspondence principle is applicable, the stresses in a linearly viscoelastic body are the same as those given in the preceding subsection for elastic media. The only stress result which will be needed for predicting

crack growth is Eq. (22) relating the stress intensity factor, N_o, to the failure stress and size of the failure zone. Recall that, by definition, N_o is the stress intensity factor for a crack with $\sigma_f \equiv 0$. This factor depends, at most, on parameters defining the geometry of the body (including instantaneous crack size and location) and on the applied stresses; in view of the earlier comment, Poisson's ratio dependence is not precluded as long as it is constant.

Turning to the prediction of displacement v along $y = 0$, we observe that this displacement close to the crack tip, Eqs. (26) and (27), meets restriction (c). For a stationary or growing crack, the extended correspondence principle yields for $t \geq t_1$:

$$v = \frac{1}{2\pi} \int_{t_1}^{t} C_v(t - \tau) \frac{\partial}{\partial \tau} \left\{ \int_{o}^{a} \sigma_f(\xi') \left[2\left(\frac{\xi}{\xi'}\right)^{1/2} - \ln \left| \frac{\sqrt{\xi'} + \sqrt{\xi}}{\sqrt{\xi'} - \sqrt{\xi}} \right| \right] d\xi' \right\} d\tau \quad . \tag{41}$$

The variable of integration τ is a generic value of time which ranges from the time, t_1, when the crack tip first reaches a point x, to the current time t; this time integration is to be performed at constant x, and therefore for moving cracks ξ must first be expressed in terms of x and τ; viz., from Eq. (5):

$$\xi = \xi(x,\tau) = a(\tau) - x \tag{42}$$

In view of the above definition of t_1,

$$\xi(x,t_1) = a(t_1) - x = 0 \tag{43}$$

and since decreasing crack size is not allowed,

$$\xi(x,\tau) \geq 0 \; ; \; \tau \geq t_1 \quad . \tag{44}$$

Also, although not explicitly shown, the length of the failure zone α and the failure stress may depend on time, τ.

If the crack is stationary we may set $t_1 = 0$, corresponding to the time at which loads are first applied to the body; Eq. (41) then applies for $x \leq a$.

The function $C_v(t)$ is defined by the equation

$$s\,\bar{C}_v \equiv \frac{4[1 - (s\bar{\nu})^2]}{s\bar{E}} \tag{45}$$

in which the bar denotes the Laplace transform (LT) of a function of time; e.g.,

$$\bar{q} \equiv \int_0^\infty e^{-st}\, q(t)\, dt \quad . \tag{46}$$

Also, $\bar{E}$ is the LT of the uniaxial relaxation modulus and $\bar{\nu}$ is the LT of the Poisson's ratio for a uniaxial relaxation test. Equation (45) can be easily established by comparing elastic stress-strain equations with the LT of those for a viscoelastic material [13]. For some problems, it may be desirable to express $C_v(t)$ in terms of the uniaxial creep compliance D(t), where

$$s\bar{D} = \frac{1}{s\bar{E}} \quad . \tag{47}$$

If Poisson's ratio is constant with the value ν, then $\bar{s\nu} = \nu$ and we can combine Eqs. (45) and (47) to find, by LT inversion,

$$C_\nu(t) = 4(1 - \nu^2)\, D(t) \quad . \tag{48}$$

Even when Poisson's ratio is not constant, Eq. (48) with $\nu = \nu(t)$ is expected to be a good approximation [1]; this result, which is based on the quasi-elastic method, can be expressed just as well using the Poisson's ratio measured in a uniaxial creep test, $\nu_c(t)$, since typically $\nu_c(t) \simeq \nu(t)$ [1].

Recall that Eq. (41) is based on an elastic solution which is valid only in the neighborhood of the crack tip. Therefore one cannot expect this viscoelastic solution to be valid for values of ξ much greater than α; this limitation does not restrict the subsequent fracture analysis as we will need the displacement only in the interval $0 \leq \xi \leq \alpha$. An additional result that will be needed is the viscoelastic version of Eq. (38) in which only the term of order $\xi^{3/2}$ is retained:

$$v \simeq -\frac{2}{3\pi} \int_{t_1}^{t} C_\nu(t - \tau)\, \frac{\partial}{\partial \tau} \left\{ \frac{\sigma_m}{\sqrt{\alpha}}\, I_2\, \xi^{3/2} \right\} d\tau \tag{49}$$

where $t \geq t_1$. All of the comments following Eq. (41) apply as well to Eq. (49) except, strictly speaking, this latter equation is restricted to the range $0 \leq \xi << \alpha$; in Appendix C we demonstrate that, in reality, Eq. (49) represents quite a good approximation for the purpose of calculating work input to the failure zone.

Finally, it should be mentioned that restriction (c) of Graham's

extended correspondence principle, which was stated early in this subsection, is overly restrictive. Namely, the product dependence of the displacement on material properties is not essential, as we shall presently show. This latter observation is particularly important to us because the elastic displacement in Eqs. (26) and (27), which has the product dependence, applies only to the neighborhood of the crack tip; whether or not this dependence exists far away from the tip probably depends on the specific problem considered, and we do not want to restrict the viscoelastic displacement solution unnecessarily. Now, following the reasoning in Graham's paper [14] and assuming restrictions (a) and (b) are met, we conclude that the LT of the viscoelastic displacement anywhere along the entire crack plane is $\bar{v} = \bar{v}_e\,[s\bar{E},\ s\bar{\nu},\ x,\ s]$ where $\bar{v}_e$ is the LT of the elastic displacement in which Young's modulus and Poisson's ratio have been replaced by $s\bar{E}$ and $s\bar{\nu}$, respectively. Explicitly,

$$\bar{v} = \int_{t_1}^{\infty} v_e[s\bar{E},\ s\bar{\nu},\ x,\ t]\ e^{-st}\ dt \tag{50}$$

where we have used the fact that the elastic displacement at the point x along the line of crack prolongation is zero until time t_1. Change the variable of integration to $\rho \equiv t - t_1$:

$$\bar{v} = e^{-st_1} \int_{o}^{\infty} v_e[s\bar{E},\ s\bar{\nu},\ x,\ \rho + t_1]\ e^{-s\rho}\ d\rho \quad . \tag{51}$$

Denoting the inverse by $\mathcal{L}^{-1}\{\ \}$, Eq. (51) yields

$$v = \mathcal{L}^{-1}\left\{\int_{o}^{\infty} v_e\ e^{-s\rho}\ d\rho\right\} H(t - t_1) \tag{52}$$

which shows that this displacement correctly vanishes for $t < t_1$. While there is no need, in principle, to assume a special form for the dependence of v_e on $s\bar{E}$ and $s\bar{\nu}$, the inversion is greatly facilitated if this displacement consists of a sum of terms, or a single term, in which the dependence on E and ν factors. Specifically, for the problem at hand we can write

$$\int_0^\infty v_e \, e^{-s\rho} \, d\rho = \frac{s\bar{C}_v}{2\pi} \bar{q} + \Delta\bar{v}_e \tag{53}$$

where $\bar{q}$ is the LT of the integral in Eq. (26), in which $\xi \equiv a(\rho + t_1) - x$; also, $\Delta\bar{v}_e$ is the LT of the higher order terms in Eq. (4). Substituting Eq. (53) into (52), neglecting Δv_e, using the convolution rule for the inversion of a product of transforms and replacing ρ by $t - t_1$ yields Eq. (41).

3. Analysis of Crack Motion

Equations for predicting time-dependent crack extension will be developed in this section; the preceding analysis plus an energy criterion for failure provide the basis for these predictions. However, we believe it will be helpful to first discuss briefly the history of events which occurs in the failure zone from the standpoint of the simplified model illustrated in Fig. 1.

Suppose an initially unstressed and unstrained body is subjected to gradually increasing load(s). The stress intensity factor in Eq. (22) will then increase in time; at any instant the length of the

failure zone must satisfy this equation, even before the left end ($\xi = \alpha$) of the zone starts to move. (If, for example, the maximum failure stress, σ_m, and the "shape" of the failure stress distribution, as defined by f in Eq. (21), remain constant, we see α, and therefore a, will grow in proportion to N_o^2.) Eventually, with increasing load, a small column of material at the left end of the failure zone will rupture and the entire failure zone will start to move to the right; the time at which this movement initiates will be called "fracture initiation time," and denoted by t_i. In many cases the time t_i will be extremely small compared to the total time for complete fracture of a body [2] and, therefore, may not be of direct practical use; prediction of the eventual crack growth behavior would then be of primary interest for establishing gross fracture times.

In developing the equations governing crack growth under various loading conditions, it is desirable to divide the analysis into two parts: (i) continuous crack growth corresponding to times $t > t_i$ and (ii) initial and intermittent crack growth corresponding to times $0 < t \leq t_i$ and to periods during which the applied loading drops below that necessary for continuous crack growth. It should be noted that the loading may vary in time in both parts (i) and (ii); however, it is assumed in the first part that the loading is at least great enough to sustain continuous motion of the entire failure zone in the direction of $+x$.

The same fracture criterion will be used in both parts. Specifically, a column of material with cross-sectional area dA

in the failure zone $0 \leq y \leq v$ is said to fail when the total work done on it by the adjacent linear continuum reaches the value $\Gamma\, dA$. (There will be no need to separately identify the failure of perfectly brittle materials. In this case $\Gamma\, dA$ could be interpreted as the mechanical work necessary to completely separate adjacent surfaces with area dA, and Γ would be the so-called "cohesive surface energy"; as indicated previously, the failure zone for this case is simply the zone in which significant forces act between atoms in adjacent crack surfaces.)

In general, the quantity Γ depends on the entire history of the force, $\sigma_f\, dA$, applied to a given column of material. Fortunately, however, there are many viscoelastic materials for which experimental and theoretical considerations indicate that Γ is at least approximately constant [2]. The quantity Γ, whether history-dependent or not, will be called fracture energy in the remainder of this paper. Equations which relate Γ to motion of the surrounding continuum are given in the next subsection. We then take up parts (i) and (ii) in separate subsections.

Calculation of Work Done on Failure Zone

The energy $\Gamma\, dA$ is equal to the work done by the upper portion ($y > 0$) of the continuum against the force, $\sigma_f\, dA$, at a fixed generic location, x, as it suffers the total vertical displacement, v_m; this displacement is defined by the condition that $\sigma_f \simeq 0$ when $v > v_m$. Thus, the work input per unit of new area is

$$\Gamma = \int_0^{v_m} \sigma_f \, dv \tag{54}$$

or, equivalently,

$$\Gamma = \int_{t_1}^{t_2} \sigma_f \frac{\partial v}{\partial t} \, dt \tag{55}$$

where vertical motion begins at t_1 and reaches v_m at t_2; note that the time derivative is taken with x held constant.

Another, more useful form with continuous crack propagation is obtained by considering the displacement in Eq. (54) to be a function of the independent variables (x,ξ), instead of (x,t), where by definition

$$\xi = \xi(x,t) \equiv a(t) - x \quad . \tag{56}$$

It is assumed here that $t_1 \leq t \leq t_2$ and $(a - \alpha) \leq x \leq a$. We select x such that it is at the crack tip when $t = t_1$; note that $\xi(x,t_1) = 0$, and $(a(t_2) - x)$ is the length of the zone of failure, α.

Equation (54) now becomes

$$\Gamma = \int_0^{\alpha} \sigma_f \frac{\partial v}{\partial \xi} \, d\xi \tag{57}$$

in which $v = v(x,\xi)$ and $da/dt > 0$.

The above change of independent variables, $(x,t) \rightarrow (x,\xi)$, may be viewed as a coordinate transformation; viz.,

$$x' = x \tag{58a}$$

$$\xi = a(t) - x \quad . \tag{58b}$$

The Jacobian determinant is found to be da/dt, and therefore Eq. (58) defines an admissible (one-to-one) transformation [13] as long as the crack velocity does not vanish.

Prediction of Continuous Crack Growth

The governing equations for crack growth will be derived by bringing together the finite stress condition, Eq. (22), the viscoelastic displacement, Eq. (41) (and Eq. (49)), and the fracture energy, Eq. (57). Even if a constitutive equation for the failure zone were known, the task of finding the solution a = a(t) to this set of nonlinear integro-differential equations would be very formidable, to say the least. There are, however, two cases when the equations greatly simplify.

The first one is for a material with infinite strength ($\sigma_m \to \infty$). It is shown in Appendix B that the exact result is the classical condition for critical stress intensity factor of a brittle material in plane strain :

$$N_o = \sqrt{\frac{\Gamma\, E(0)}{\pi[1 - \nu^2(0)]}} \tag{59}$$

where $E(0)$ and $\nu(0)$ are the initial values of relaxation modulus and Poisson's ratio. The stress predicted by this equation is unrealistically high compared to the values at which cracks can be made to propagate in viscoelastic materials [2], and moreover the crack velocity is undefined. Except for representing a limiting situation, this case of infinite strength at the tip, therefore, is of little practical interest.

The second case is based on a certain property of the creep compliance which exists for most polymeric materials. Specifically, a double-logarithmic plot of creep compliance (e.g., in simple shear or uniaxial tension) has small curvature over most, if not all, of its range of variation [e.g., 1 , 16]; the specific meaning of "small" will be brought out later in the analysis. The creep compliance, $C_v(t)$, which is defined by Eq. (45), can be expected to have small curvature when $D(t)$ has this property since Poisson's ratio typically is a very weak function of time; see also Eq. (48). As one example, the creep compliance in the glass-to-rubber transition range for Solithane 50/50 [6] under uniaxial tension is shown in Fig. 4; this material is an unfilled, crosslinked, amorphous polymer. The compliance of particulate filled-polymers (e.g., solid propellant) in the glass-to-rubber transition range and the compliance of plastics typically vary over a greater range of log t and have even less

curvature than seen in Fig. 4. In view of the generality of this behavior and the analytical simplification it produces, we shall concern ourselves with this case in the remainder of this subsection.

As noted previously, α and σ_f may be functions of time, although this dependence is not explicitly shown in Eqs. (41) and (49). However, it will be assumed that the time it takes for the crack to propagate an amount α is small enough that α and σ_f are essentially timewise constant during this brief period, denoted as $t_2 - t_1$. Note that Eq. (18) (or Eq. (22)) implies N_o must be essentially constant during this same period; nevertheless, it is important to realize that N_o may vary either weakly or strongly with time during the total period of crack growth. Additionally, we assume $a(t)$ can be linearized during the short period $t_2 - t_1$; thus with $0 \leq \xi \leq \alpha$,

$$a(t) \simeq a(t_1) + (t - t_1)\dot{a} \tag{60a}$$

and using Eq. (42),

$$\xi(x,\tau) = a(\tau) - x \simeq (\tau - t_1)\dot{a} \tag{60b}$$

$$\xi(x,t) = a(t) - x \simeq (t - t_1)\dot{a} \tag{60c}$$

where $a(t_1) = x$ and $\dot{a}$ is the tip velocity at the generic time t_1. We consider t_1 to be a function of x since it is the time at which the crack tip reaches the fixed location x.

Reduction of Convclution Integrals: The above simplifications will be used to reduce the (convolution) time integral in displacement Eq. (49) to a simple product form; extension of this result to exact displacement, Eq. (41), is then made.

After changing the time variables in Eq. (49) by using the definitions

$$\rho \equiv \tau - t_1 \tag{61a}$$

$$\Delta t \equiv t - t_1 \tag{61b}$$

we find

$$v \simeq - \frac{2\,\sigma_m\, I_2}{3\,\pi\,\sqrt{\alpha}}\,\xi^{3/2}\, C_{ef}\,(\Delta t)\, H(\xi) \tag{62a}$$

where

$$\xi = \xi(x,t) \simeq \Delta t\, \dot{a} \tag{62b}$$

and we have defined an "effective" compliance,

$$C_{ef}(t) \equiv \frac{3}{2}\, t^{-3/2} \int_0^t C_v(t - \rho)\, \rho^{1/2}\, d\rho \quad . \tag{63}$$

Now convert Eq. (63) to a logarithmic time scale using the definitions (where $\log \equiv \log_{10}$):

$$\rho_v \equiv \rho/t$$

$$L \equiv \log t$$

$$\ell \equiv \log(1 - \rho_v)$$

$$\hat{C}_v(L) \equiv C_v(t) \quad . \tag{64}$$

Note that $\hat{C}_v(L)$ is simply the creep compliance expressed in terms of logarithmic time. Equation (63) becomes

$$C_{ef}(t) = \frac{3}{2} (\ln 10) \int_{-\infty}^{0} \hat{C}_v(L + \ell) \left\{10^{\ell} [1 - 10^{\ell}]^{1/2}\right\} d\ell. \tag{65}$$

The quantity in curly brackets will be called a weighting function and denoted $w_{3/2}$; it is plotted in Fig. 5 over its major range of variation. Recognizing that the creep compliance $\hat{C}_v$ is an increasing function of its argument, and observing the rather narrow range for which $w_{3/2}$ differs appreciably from zero, we conclude that $C_{ef}(t)$ depends on only a small part of the total creep compliance curve (e.g., Fig. 4). Since L is the current value of logarithmic time, Eq. (65) shows that the influencial part of the creep compliance is in the (approximately) 1.2 decade range from (log t - 1.2) to log t. We assume that over this 1.2 decade range the creep compliance can be represented by the power law

$$C_v(t) = C_1 t^n \quad . \tag{66}$$

Somewhat arbitrarily, we select the exponent n to be the log-log slope of the creep compliance at the point $L - 0.48$, which is near the centroid of the weighting function. Inasmuch as $L - 0.48 = \log t - \log 3.0 = \log (t/3.0)$, we see n is the slope of a line drawn tangent to a double logarithmic plot of $C_v(t)$ at $t/3$. The coefficient C_1 is the value of compliance where this tangent line intercepts the $\log t = 0$ axis.

The actual value of effective compliance is now readily derived by substituting power law Eq. (66) into Eq. (63), and treating n and C_1 as constants in performing the integration; there results

$$C_{ef}(t) \simeq \lambda_n C_1 t^n \tag{67}$$

or, equivalently,

$$C_{ef}(t) \simeq C_v(\lambda_n^{1/n} t) \tag{68}$$

where

$$\lambda_n \equiv \frac{3\sqrt{\pi}\,\Gamma(n+1)}{4(n+\frac{3}{2})\,\Gamma(n+\frac{3}{2})} \tag{69}$$

and

$$\Gamma(n) \equiv \int_0^\infty t^{n-1} e^{-t}\, dt \tag{70}$$

is the Gamma function with argument n. The factor λ_n is plotted in Fig. 6 for the range of n exhibited by polymers (i.e., $0 \leq n \leq 1$); for most polymers $0 \leq n \leq 0.5$, with filled polymers and plastics

usually having n values at the low end of this range. Consequently, the effective compliance is commonly very close to the creep compliance itself.

Returning to the displacement Eq. (62a), we see that it can be written in the simple form

$$v \simeq - \frac{2 \sigma_m I_2}{3 \pi \sqrt{\alpha}} \xi^{3/2} \lambda_n C_1 \Delta t^n H(\xi) \tag{71}$$

and using Eqs.(62b) and (66),

$$v \simeq - \frac{2 \sigma_m I_2}{3 \pi \sqrt{\alpha}} \xi^{3/2} C_v(\tilde{t}) H(\xi) \tag{72a}$$

where

$$\tilde{t} \equiv \lambda_n^{1/n} \xi / \dot{a} \quad . \tag{72b}$$

Equation (72) is identical to the elastic displacement except $C_v(\tilde{t})$ appears in place of C_e.

This simple result is easily generalized to the case in which higher order terms are retained in the displacement expansion. Namely, suppose the elastic solution is represented by the sum,

$$v = \sum_r v_r H(\xi) \tag{73}$$

in which

$$v_r = A_r \xi^r C_e \tag{74}$$

where $r > 1$ and A_r is essentially constant during the period $(t_2 - t_1)$

required for the crack to propagate a distance α. The viscoelastic solution to each term for $t_2 \geq t \geq t_1$ can be written in the form

$$v_r = A_r \, \xi^r \, C_{ef}^{(r)} \, (\Delta t) \tag{75}$$

where the r^{th} effective compliance is

$$C_{ef}^{(r)}(t) \equiv r \, t^{-r} \int_o^t C_v(t - \rho) \, \rho^{r-1} \, d\rho \quad . \tag{76}$$

When this compliance is expressed using a logarithmic time scale through definitions in Eq. (64) we obtain a result which is identical to Eq. (65) except the weighting function w_r, say, must be changed using the substitution,

$$10^{\ell}[1 - 10^{\ell}]^{1/2} \rightarrow \frac{2}{3} \, r \, 10^{\ell}[1 - 10^{\ell}]^{r-1} \equiv w_r \tag{77}$$

The weighting function for $r = \frac{5}{2}$ is shown in Fig. 5, and is seen to be close to that for $r = \frac{3}{2}$. Indeed, this function is relatively insensitive to r; for example, the maximum occurs at

$$\ell = - \log r \tag{78a}$$

with the value

$$w_r(\max) = \frac{2}{3} \, (1 - \frac{1}{r})^{r-1} \tag{78b}$$

and

$$w_r(\max) \rightarrow \frac{2}{3e} \approx 0.25 \quad \text{as} \quad r \rightarrow \infty \quad . \tag{78c}$$

The general shape of each w_r is the same as those in Fig. 5. It is

important to realize that even for r quite large the essential part of the weighting function lies in the same ℓ-range as the curves in Fig. 5; for example, with $r = 10$ the maximum is at $\ell = -1$ and has the value $w_{10}(\max) \approx 0.26$.

Thus, the effective compliance can be evaluated quite accurately for a wide range of r using Eq. (66) with constants found from the tangent to the log-log plot of $C_v(t)$ at $t/3$. When this power law is substituted into Eq. (76) we find

$$C_{ef}^{(r)}(t) = \lambda_{nr} C_1 t^n \tag{79}$$

where

$$\lambda_{nr} = \frac{r\,\Gamma(r)\,\Gamma(n+1)}{(n+r)\,\Gamma(n+r)} \tag{80}$$

The coefficient λ_{nr} reduces to Eq. (69) when we set $r = \frac{3}{2}$. This compliance coefficient is drawn in Fig. 6 for four different values of r; λ_{nr} for $r = 1$ is shown because the exponent is a lower bound, although values of r less than $\frac{3}{2}$ are not expected to appear in a series expansion of the exact displacement in view of the analysis in Section 2.

The relative insensitivity of λ_{nr} to r, especially for the usual range of n for polymers ($0 \leq n \leq 0.5$), leads immediately to a simple solution to the viscoelastic displacement. For example, suppose the elastic displacement, Eq. (27), can be approximated by a three-term series

$$v \simeq \xi^{1/2}[A_{3/2}\xi + A_{5/2}\xi^2 + A_{7/2}\xi^3]\, C_e\, H(\xi) \quad . \qquad (81a)$$

Then according to Eqs. (75) and (79) an approximate viscoelastic solution is

$$v \simeq \xi^{1/2}[A_{3/2}\xi + A_{5/2}\xi^2 + A_{7/2}\xi^3]\, \lambda_n\, C_1 \Delta t^n\, H(\xi) \qquad (81b)$$

and using Eqs.(62b), (66), and (72b),

$$v \simeq \xi^{1/2}[A_{3/2}\xi + A_{5/2}\xi^2 + A_{7/2}\xi^3]\, C_v(\tilde{t})\, H(\xi) \quad . \qquad (81c)$$

We have replaced the individual coefficients λ_{nr} with λ_n (corresponding to $r = \frac{3}{2}$) on the assumption that the first term in the series is the largest, and therefore λ_n is more appropriate than a simple average of the three coefficients. We now replace the series in Eq. (81c) by the original expression, Eq.(27), and obtain the important result,

$$v \simeq \frac{C_v(\tilde{t})}{2\pi} H(\xi) \int_0^{\alpha} \sigma_f(\xi') \left\{ 2\left(\frac{\xi}{\xi'}\right)^{1/2} - \ln\left|\frac{\sqrt{\xi'} + \sqrt{\xi}}{\sqrt{\xi'} - \sqrt{\xi}}\right| \right\} d\xi' \qquad (82)$$

where $\tilde{t}$ is given by Eq. (72b).

Although Eq. (82) is considerably simpler than the exact displacement, Eq. (41), it is believed that it is sufficiently accurate for our purposes regardless of the nature of the failure stress distribution. We intend to use this displacement to calculate only the work done on the total failure zone, Eq. (57); this computation is, of course, an averaging process and requires the displacement just in the range of $0 \leq \xi \leq \alpha$. Moreover, by assuming

several different realistic functions for σ_f it is shown in Appendix C that even the one-term representation, Eq. (72a), is quite good for this purpose.

In further support of the accuracy of Eq. (82), let us consider a few simple examples of displacement predictions. First, suppose σ_f is independent of ξ; viz., $\sigma_f \equiv \sigma_m$. The exact elastic displacement is found from Eq. (26) to be

$$v = \frac{A}{2}\left[2\sqrt{\eta} - (1 - \eta)\ \ln\left|\frac{1 + \sqrt{\eta}}{1 - \sqrt{\eta}}\right|\right] H(\xi) \tag{83a}$$

where $\eta \equiv \xi/\alpha$ and

$$A \equiv C_e\ \sigma_m\ \alpha/\pi \quad . \tag{83b}$$

Expanding the logarithm in a power series yields for $0 \leq \eta \leq 1$:

$$v = 2A\ \eta^{1/2}\left[\frac{1}{3}\ \eta + \frac{1}{15}\ \eta^2 + \frac{1}{35}\ \eta^3 + \frac{1}{63}\ \eta^4 + \cdots\right] H(\xi) \tag{83c}$$

As a measure of the error in Eq. (83c) if only three terms are retained (as in Eq. (81a)), we shall calculate the ratio of this displacement, denoted by v_3, to the exact displacement, Eq. (83a), at $\eta = 1$:

$$\frac{v_3(1)}{v(1)} \simeq 0.86 \quad . \tag{83d}$$

If only the first term is retained in Eq. (83c), denoted by v_1, then

$$\frac{v_1(1)}{v(1)} \simeq 0.67 \quad . \tag{83e}$$

As a further comparison we calculate the ratio $v_1(1)/v(1)$ given the two functions

$$\text{(i)} \quad \sigma_f = \sigma_m[1 - \eta^2]$$

$$\text{(ii)} \quad \sigma_f = \sigma_m[1 - \eta] \quad . \tag{84a}$$

Equation (38) may be used to find the one-term approximation, $v_1(1)$, with Eq. (26) still used to find the exact displacement $v(1)$; the result is

$$\text{(i)} \quad v_1(1)/v(1) = 0.80$$

$$\text{(ii)} \quad v_1(1)/v(1) = 1.33 \tag{84b}$$

The first result, Eq. (83d), although representing only a 14% error in displacement at the end of the failure zone, could be reduced even further by evaluating the three coefficients differently; e.g., a least squares method could be used. The above results (and Appendix C) for a one-term representation give evidence that the essential features of the displacement at the boundary of the failure zone are embodied in the function $\xi^{3/2}$.

Calculation of Work Done on the Failure Zone: Equation (57) will be evaluated using displacement Eq. (82). First, we define an auxiliary function v_α,

$$v_\alpha \equiv \frac{C_v(\tilde{t}_\alpha)}{C_v(\tilde{t})}\, v \tag{85}$$

where v is the displacement in Eq. (82) and

$$\tilde{t}_\alpha \equiv \lambda_n^{1/n}\, \alpha/\dot{a} \quad . \tag{86}$$

Also, by definition, the coefficient C_1 and exponent n used in $C_v(\tilde{t}_\alpha)$ and Eq. (86) are to be obtained from the tangent to the double logarithmic plot of the creep compliance $C_v(t)$ at the time $\alpha/3\dot{a}$; note that $\alpha/\dot{a}$ is the time the crack tip takes to propagate the distance α.

Now, divide the work input into two parts by adding and subtracting v_α; thus

$$\Gamma = \Gamma_a + \Gamma_b \tag{87a}$$

where

$$\Gamma_a \equiv \int_o^\alpha \sigma_f(\xi)\, \frac{\partial v_\alpha}{\partial \xi}\, d\xi \tag{87b}$$

$$\Gamma_b \equiv \int_o^\alpha \sigma_f(\xi)\, \frac{\partial}{\partial \xi}\, (v - v_\alpha)\, d\xi \quad . \tag{87c}$$

It will be shown that the second integral is relatively small while the first one reduces to a simple function of the stress intensity factor.

The Integral Γ_b: Use of Eq. (85) yields

$$\Gamma_b = \int_o^\alpha \sigma_f(\xi)\, \frac{\partial}{\partial \xi} \left\{ \left[\frac{C_v(\tilde{t})}{C_v(\tilde{t}_\alpha)} - 1 \right] v_\alpha \right\} d\xi \quad . \tag{88a}$$

Integrate-by-parts and use the fact that $v_\alpha = 0$ at $\xi = 0$ and $C_v(\tilde{t}_\alpha) = C_v(\tilde{t})$ at $\xi = \alpha$:

$$\Gamma_b = \int_o^\alpha \frac{\partial \sigma_f}{\partial \xi} \left[\frac{C_v(\tilde{t})}{C_v(\tilde{t}_\alpha)} - 1\right] v_\alpha \, d\xi \quad . \tag{88b}$$

We see that Γ_b vanishes identically for two important limit cases: (i) constant failure stress distribution, $\sigma_f \equiv \sigma_m$; and (ii) elastic continuum. It should be added that in both of these cases the material in the failure zone may be highly nonlinear and viscoelastic without affecting the vanishing of Γ_b. For cases other than the above two we return to Eq. (88a) and note that the term in curly brackets is small in magnitude when v_α is large (i.e., when $\xi \approx \alpha$) and vice-versa (i.e., when $\xi \approx 0$). Figure 7 shows the entire term in curly brackets (normalized with respect to the displacement at the end of the failure zone, $v(\alpha)$) when the displacement variation is given by $\xi^{3/2}$; this use of a one-term representation of displacement is not crucial to the argument as other cusp-type displacement variations would lead to the same general behavior shown in Fig. 7.

We have used the same constants (n, C_1) in both compliances in Eq. (88a), which yields

$$\left[\frac{C_v(\tilde{t})}{C_v(\tilde{t}_\alpha)} - 1\right] v_\alpha = - \left[1 - \eta^n\right] \eta^{3/2} \, v(\alpha) \quad . \tag{89a}$$

Now, Γ_b is the work done by σ_f acting through a displacement equal to

the entire quantity in Eq. (89a). By comparison, Eq. (87b) shows that Γ_a is the work done by σ_f acting through the displacement v_α,

$$v_\alpha = \eta^{3/2}\, v(\alpha) \quad . \tag{89b}$$

Examination of the displacements in Fig. 7 reveals clearly that $\Gamma_a >> \Gamma_b$ unless σ_f acts mainly in the neighborhood of $\eta = 0$. Such behavior of σ_f cannot exist in view of the definition of the failure zone; viz., α is defined as the distance over which only significant values of σ_f act, and if σ_f acted only at the far left of Fig. 7, α would be reduced accordingly. However, it is of interest to point out that for even the rather rapidly decaying stress $\sigma_f = \sigma_m(1 - \eta^{1/2})$ the ratio Γ_b/Γ_a is $n/(n + 2)$ and this ratio is less when the actual displacement variation is used in the calculation instead of $\eta^{3/2}$. (If one wished to retain Γ_b, its evaluation using even a crude estimate of σ_f probably would be adequate considering its smallness.)

As one final point concerning Γ_b, we should mention that quantities n and C_1 generally will vary with η, rather than being constant as assumed in deriving Eq. (89a). However, by changing Eq. (88b) to a logarithmic scale, $\log \eta$, and using arguments analogous to those used to derive Eq. (67), it can be shown that Γ_b is essentially independent of $\tilde{t}$ except for the range $10^{-2}\, \tilde{t}_\alpha \lesssim \tilde{t} \lesssim \tilde{t}_\alpha$; this observation together with the typically weak dependence of C_1 and n on $\log t$ justifies our use of Eq. (89a).

The Integral Γ_a: We shall write out Γ_a, Eq. (87b), by using

Eq. (82) and definition Eq. (85); after performing the differentiation there results, finally,

$$\Gamma_a = \frac{C_v(\tilde{t}_\alpha)}{2\pi} \int_o^\alpha \int_o^\alpha \frac{\sigma_f(\xi)\ \sigma_f(\xi')}{\sqrt{\xi}\ \sqrt{\xi'}} \left\{ \frac{\xi}{\xi - \xi'} \right\} d\xi'\ d\xi \quad . \tag{90a}$$

Note that

$$\frac{\xi}{\xi - \xi'} = \frac{1}{2} + \frac{1}{2} \left(\frac{\xi + \xi'}{\xi - \xi'} \right) \quad . \tag{90b}$$

Substitution of Eq. (90b) into (90a) and use of Eq. (18) for the stress intensity factor yields

$$\Gamma_a = \frac{\pi}{4} C_v(\tilde{t}_\alpha)\ N_o^2 + Z \tag{90c}$$

where

$$Z \equiv \frac{C_v(\tilde{t}_\alpha)}{4\pi} \int_o^\alpha \int_o^\alpha \frac{\sigma_f(\xi)\ \sigma_f(\xi')}{\sqrt{\xi}\ \sqrt{\xi'}} \left\{ \frac{\xi + \xi'}{\xi - \xi'} \right\} d\xi'\ d\xi \quad . \tag{90d}$$

The integral Z is identically zero. This result is clearly seen by referring to Fig. 8 and observing that the integrand, $\mathcal{L}(\xi,\xi')$, say, is skew-symmetric with respect to the line $\xi = \xi'$; viz., by direct substitution one finds

$$\mathcal{L}(\xi_1,\xi_1') = -\mathcal{L}(\xi_2,\xi_2') \quad . \tag{90e}$$

Governing Equations for Crack Growth: Neglecting Γ_b on the basis of the above arguments and bringing together Eqs. (87a) and (90c)

yields the principal result of this paper:

$$C_v(\tilde{t}_\alpha) = \frac{4\Gamma}{\pi N_o^2} \tag{91}$$

This equation is identical to that for the critical stress intensity factor of an elastic material (see Eq. (59)) except the linear viscoelastic creep compliance $C_v(\tilde{t}_\alpha)$ appears in place of the elastic constant, $4(1 - \nu^2)/E$. For completeness we record here the definition of $\tilde{t}_\alpha$:

$$\tilde{t}_\alpha \equiv \lambda_n^{1/n}\, \alpha/\dot{a} \tag{92a}$$

where α is found from Eq. (22),

$$\alpha = \frac{\pi^2 N_o^2}{\sigma_m^2 I_1^2} \tag{92b}$$

and $\lambda_n^{1/n}$ is obtained from Fig. 6, with the value of n simply related to creep compliance,*

$$n = \frac{d \log C_v(t)}{d \log t} \tag{92c}$$

at the time $t = \alpha/3\dot{a}$. Experimental and theoretical determination of fracture properties Γ and $\sigma_m I_1$, and their possible velocity dependence, will be discussed a little later; for the time being we shall treat them as known quantities.

The general character of continuous crack propagation in viscoelastic media can now be described. First, we note that $C_v(\tilde{t}_\alpha)$ is a continuous, monotonic, increasing function of $\tilde{t}_\alpha$ having

*In most problems, the value $\lambda_n^{1/n} = 1/3$ obviously will be acceptable.

the range of variation,

$$C_v(0) \leq C_v(\tilde{t}_\alpha) \leq C_v(\infty) \quad . \tag{93}$$

Thus, Eq. (91) admits a single-valued continuous solution $\tilde{t}_\alpha$, given N_o and Γ, for the following range of stress intensity factors

$$N_{oe} < N_o < N_{og} \tag{94a}$$

where

$$N_{oe} \equiv \sqrt{\frac{4\,\Gamma}{\pi\, C_v(\infty)}} \tag{94b}$$

and

$$N_{og} \equiv \sqrt{\frac{4\,\Gamma}{\pi\, C_v(0)}} \quad . \tag{94c}$$

These limiting stress-intensity factors are identical to so-called critical stress-intensity factors of elastic media having elastic constants $4(1 - \nu^2(\infty))/E(\infty)$ and $4(1 - \nu^2(0))/E(0)$, respectively; the relation between $C_v(\infty)$, $C_v(0)$ and these elastic constants follows from application of the initial and final value theorems of Laplace transform theory [17] to Eq. (45).

Henceforth, N_{oe} and N_{og} will be called the <u>equilibrium</u> and <u>glassy</u> factors, respectively; the equilibrium factor for a non-crosslinked polymer is zero since $C_v(\infty) = \infty$.

Returning to Eqs. (91) and (92), we see the behavior described above implies the instantaneous crack tip velocity $\dot{a}$ is a monotonically increasing function of N_o in the range in Eq. (94);

although Γ and $\sigma_m I_1$ may depend on velocity it is doubtful this dependence would alter this general behavior. As N_o approaches N_{og} from below, $\dot{a}$ becomes unbounded, while as N_o approaches N_{oe} from above $\dot{a}$ approaches zero. It is concluded, therefore, that a crack will not propagate if $N_o \leq N_{oe}$ and will propagate at high velocities (limited of course by effects of wave action which have not been taken into account in this paper) when $N_o \geq N_{og}$.

Another point of interest is that instantaneous tip velocity depends on the current value of N_o but not on past values. Recall also that $\dot{a}$ is actually the velocity <u>normal</u> to the curve defining the crack tip, and consequently Eq. (91) enables one to compute the time-dependent shape and size of a crack in terms of <u>local</u> stress intensity factors.

In order to solve Eq. (91) explicitly for tip velocity it may be desirable to reintroduce the power-law form $C_v(t) = C_1 t^n$; Eqs. (91) and (92) then yield, with $\dot{a} \equiv da/dt$:

$$\frac{da}{dt} = \left\{ \frac{C_1 \lambda_n \pi^{(2n+1)}}{4 \Gamma} \right\}^{1/n} \frac{N_o^{2(1+1/n)}}{\sigma_m^2 I_1^2} \tag{95}$$

(In the development of the theory, $\dot{a}$ was defined to be the velocity at the time, t_1, which is the time at which the crack reaches a generic location x; for notational simplicity we now drop the subscript "1" on the time variable.) In general, this is a first order nonlinear differential equation for crack length. If n is not constant, it has to be expressed in terms of N_o and $\dot{a}$ through

Eqs. (92b) and (92c). (In solving Eq. (95) numerically, a considerable reduction in computational time may be achieved by letting n be piecewise constant over approximately one-decade intervals in $\alpha/\dot{a}$, depending on the amount of curvature in the log-log plot of creep compliance; this is especially true when Eq. (95) admits an analytical, closed-form solution with n constant.)

The solution of Eq. (91) may be facilitated by incorporating the initial value of compliance, $C_v(0)$, in the analytical representation of $C_v(t)$; we do this by means of the generalized power law:

$$C_v(t) = C_o + C_2 t^m \tag{96}$$

where $C_o \equiv C_v(0)$; m and C_2 are, respectively, the slope and the log $t = 0$ intercept of a line drawn tangent to a double-logarithmic plot of $[C_v(t) - C_o]$ at time t. The main advantage of this representation over simple power law Eq. (66) is that m and C_2 are constant over many decades of time for numerous plastics and elastomers [1]; for example, the above form of power law fits the uniaxial data in Fig. 4 extremely well for $-\infty < \log t \tilde{<} -2$; in fact, except for a small portion of the curve close to $\log t = -2$, the entire compliance can be represented by the generalized power law up to its intersection with $D(\infty)$ and by the constant $D(\infty)$ at greater times. (Observe that the condition of small curvature used in developing the theory (e.g., Eq. (67)), which requires the slope n to be essentially constant over approximately 1.2-decade intervals, is not particularly well satisfied close to $\log t = 2$. It is important

to realize that this curvature will produce some error in Eq. (91) only when $\log (\alpha/3\dot{a}) \simeq 2$, but will not cause error at other velocities.)

One can easily show that if generalized power law Eq. (96) had been used in the development of the theory, instead of Eq. (66), Eq. (91) still would have been obtained. However, one must replace n by m in Eqs. (92a) and (92c) and in Fig. 6; also, replace $C_v(t)$ by $[C_v(t) - C_o]$ in Eq. (92c). We now solve Eq. (91) for tip velocity after drawing upon Eq. (96) and definition Eq. (94c):

$$\frac{da}{dt} = \left\{\frac{C_2 \lambda_m \pi^{(2m+1)}}{4\Gamma\left[1 - \frac{N_o^2}{N_{og}^2}\right]}\right\}^{1/m} \frac{N_o^{2(1+1/m)}}{\sigma_m^2 I_1^2} \qquad (97)$$

for $N_o^2 < N_{og}^2$. We see that when $N_o^2/N_{og}^2 << 1$ this result reduces to Eq. (95); for this range we may set $C_2 = C_1$ and $m = n$. Equation (97) also shows clearly that the velocity becomes unbounded when N_o approaches N_{og} from below.

Fracture Properties: The basic Eq. (91) was derived without explicitly imposing any significant restrictions on the nature of the failure stress, σ_f. Now we shall deduce some special, but still relatively general, representations in order to be able to make explicit predictions of crack growth and/or determine pertinent fracture properties from experimental data.

First it should be pointed out that the assumed geometry of the crack cross-section, Fig. 1, probably limits us to functions

$\sigma_f(\xi)$ which are either independent of ξ or are decreasing functions of ξ. For if σ_f increased appreciably with ξ (such as for a metal with significant strain hardening), the continuum adjacent to the failure zone would be subjected to stresses outside of its range of linear viscoelasticity, thereby invalidating a basic assumption of the theory. This limitation is <u>not</u> believed to be a serious one for most filled and unfilled polymers; certainly the theory will be suspect for some materials, such as natural rubber in which stress- and rate-dependent crystallization forms a strong, anisotropic crack tip reinforcement [2]. On this basis it will be assumed that the maximum value of σ_f, which is denoted by σ_m, occurs at the tip or at least very close to it.

Let us now determine the principal geometric and mechanical variables affecting the dimensionless failure stress distribution $f(\equiv \sigma_f/\sigma_m)$, at a generic location, ξ. In general, this stress will depend on the displacement v at ξ as well as the time variation of displacement as it increases from zero to the maximum value v_m at $\xi = \alpha$. This time variation of displacement is defined by the tip velocity $\dot{a}$ (which already has been assumed constant during the time an element of material is stretched from its initial length at $\xi = 0$ to complete failure at α), the shape of the interface between the linear continuum and failure zone, and the maximum displacement v_m; we shall express the interface shape using the single parameter $\mathscr{S}$, which is intended to represent the set of all values of v/v_m over $0 \leq \xi \leq \alpha$. The rate at which the tensile stress

in the x-direction within the failure zone decreases from its value of $\sigma_x(o)$ ($= \sigma_y(o)$) at $\xi = 0$ to zero could affect the rate of degradation and, therefore, σ_f; e.g., the triaxial tensile stress state near the tip may facilitate the production of cavities in the failure zone for some materials. It will be assumed that this effect is determined by the overall failure zone dimensions, v_m and α, tip velocity, $\dot{a}$, and interface shape $\mathcal{S}$.

One might also argue that the crack tip thickness d_i (see Fig. 3) is not a constant, and therefore should be explicitly included in the set of parameters affecting f. However, implicit in the assumption of linear viscoelastic behavior for the material outside of the failure zone is that the strains are small, and this restriction includes the strain at the tip, $\xi = 0$; within this context d_i is essentially constant and no further mention of this thickness need be made.

On the basis of the above remarks and dimensional considerations, the dimensionless distribution f can be written as follows:

$$f = F\left(\frac{v}{v_m}, \mathcal{S}, \frac{\alpha}{v_m}, \frac{\dot{a}\,\tau_j}{\alpha}\right) \tag{98a}$$

where τ_j ($j = 1,2,\ldots,N$) are N time-constants defining the rate-dependence of the failing material through bond failure and/or relaxation processes; note that each one of the associated nondimensional parameters is the ratio of the time constant to the time the crack tip takes ($\alpha/\dot{a}$) to propagate the distance α. The

parameter α/v_m reflects primarily the influence of the triaxial stress state on the degradation process.

In order to establish the variables affecting the maximum stress σ_m, consider a material point along the line of crack prolongation. As the crack tip approaches, the stresses $(\sigma_x, \sigma_y, \sigma_z)$ at this point approach $(\sigma_m, \sigma_m, \sigma_z)$, where

$$\sigma_z = \int_0^t \nu(t-\tau) \frac{\partial(\sigma_x + \sigma_y)}{\partial\tau} d\tau + \int_0^t E(t-\tau) \frac{\partial \varepsilon_z}{\partial\tau} d\tau \ . \quad (98b)$$

Strictly speaking σ_z depends on stress history as shown in Eq. (98b). However, considering the relative insensitivity of Poisson's ratio to time [1] and the fact that $\varepsilon_z \simeq 0$ in the neighborhood of the crack tip, this dependency will be neglected; hence $\sigma_z \simeq \sigma_m$.

With this observation in mind and using the previously stated assumption that the material is linearly viscoelastic outside of the failure zone, and therefore is undamaged, we conclude that σ_m is independent of stress history; σ_m may, however, depend on tip velocity. Thus

$$\sigma_m = \sigma_m\left(\frac{\dot{a}}{\alpha}\tau_j\right) \ . \quad (98c)$$

It is of interest to mention that the above representation of $\sigma_f = \sigma_m F$ contains as a special case the fracture theory of Barenblatt et al.[18], which is based on the application of rate process theory to the failure zone in an otherwise linearly elastic material. However, we shall <u>not</u> use their special form of σ_f as it

is derived from a rate equation for bond failure which is probably over-simplified [2] and also predicts the physically incorrect result of a non-zero tip velocity for a vanishingly small stress intensity factor; while such behavior could exist in noncrosslinked polymers above their glass-transition temperature, they do not satisfy the elasticity assumption made by Barenblatt et al.[18] when $\dot{a} \to 0$.

Returning to the discussion leading up to Eqs. (98a) and (98c), we may conclude that the fracture energy (which is the work done by σ_f acting through the displacement v_m) depends, at most, on the nondimensional parameters shown in Eq. (98a) except for v/v_m; viz.,

$$\Gamma = \Gamma(\mathscr{S}, \frac{\alpha}{v_m}, \frac{\dot{a}\,\tau_j}{\alpha}) \quad . \tag{99}$$

The quantities Γ, σ_m, I_1, and F, by themselves or in combination, will be called <u>fracture properties</u>. For the sake of argument, let us now suppose that these fracture properties, as well as $C_v(t)$, are given functions of their arguments. Equations (91), (92), and Eq. (82) provide a set of five equations from which the five quantities n, $\tilde{t}_\alpha$, α, $\dot{a}$, and v can be found, in principle, given N_o; note that the shape, $\mathscr{S}$, is defined by the variation of v with ξ through Eq. (82). It is therefore concluded that the <u>instantaneous</u> crack tip velocity depends on only the <u>instantaneous</u> stress intensity factor; neither the history of this factor nor the history of the stresses in the continuum enter.

This conclusion has an important practical implication. Suppose that the function $N_o = h(\dot{a})$ has been obtained experimentally over the

velocity range of interest. Then to predict crack growth due to a stress intensity factor which has different time-dependence than used in the experimental determination of $h(\dot{a})$, one does not have to introduce any new functions or fracture theory per se. Rather, all one need do is integrate the first order differential equation $N_o = h(\dot{a})$, where N_o may possibly depend on $\dot{a}$ as well as other time-dependent parameters. Of course, use of the previously derived theoretical relationships may greatly facilitate the evaluation of $h(\dot{a})$ from experimental data (especially if Γ and $\sigma_m I_1$ are constant) and simplify the determination of its dependence on such important factors as chemical aging and temperature; incorporation of these factors will be discussed shortly. For the three materials studied later in Section 4 it is found that Γ and $\sigma_m I_1$ can indeed be taken as constants; this result will be seen to provide a simple analytical representation of $h(\dot{a})$ in terms of creep compliance and enable some rather useful conclusions to be drawn concerning crack growth and failure under realistic loading conditions.

Finally, it should be clear that if only the function $h(\dot{a})$ is known, it is not possible to establish the separate fracture properties appearing in the theory. For example, we could arbitrarily assume $F = 1$ (or $I_1 = 2$) and select any constant value for σ_m and still adjust the theory, Eq. (91), so as to fit the function $f(\dot{a})$; this fitting would be accomplished by absorbing as much velocity dependence in Γ as necessary by setting $N_o = h$ and combining Eqs. (91) and (92) so as to find Γ from the equation,

$$\Gamma = \frac{\pi}{4} h^2 C_v(\lambda_n^{1/n} \alpha/\dot{a}) \tag{100a}$$

where

$$\frac{\alpha}{\dot{a}} = \frac{\pi^2 h^2}{\dot{a} \sigma_m^2 I_1^2} \tag{100b}$$

and n is defined in Eq. (92c). Unless $\sigma_m I_1$ is actually constant and its value correctly chosen, Γ as given by Eq. (100a) cannot be interpreted as true fracture energy. On the other hand, if both h and α are determined experimentally as functions of $\dot{a}$, Eq. (100a) yields the actual fracture energy after substituting these two functions. Then Eq. (100b) can be used to find $\sigma_m I_1$ in terms of $\dot{a}$.

We are thus led to an important conclusion concerning fracture experiments. If it is desired to use these experiments to establish the rate dependence of Γ and $\sigma_m I_1$, if indeed any exists, one must measure <u>both</u> crack velocity and failure zone length as functions of N_o.

<u>Effect of Environmental Changes and Aging</u>: The creep compliance C_v and fracture properties Γ and $\sigma_m I_1$ which appear in the basic fracture Eqs. (91) and (92) can be expected, in general, to vary with the environment through, for example, dependence on temperature and relative humidity. These properties may also vary directly with age due to such phenomena as post cure reactions and oxidation. As long as the resulting changes in C_v, Γ, and $\sigma_m I_1$ are relatively small in the generic time interval $\alpha/\dot{a}$, we can incorporate this time

variation in properties directly into Eqs. (91) and (92), as well as Eqs. (95) and (97), without having to alter the form of the equations; integration of the appropriate equation, taking into account the time-varying properties, will yield instantaneous crack size as a function of environment and aging histories.

As a point of caution it should be recalled that the crack propagation theory was developed under the assumption that N_o is independent of viscoelastic properties of the continuum. With sufficiently rapid changes in the environment and/or spacially nonuniform aging, the resulting inhomogeneity may give rise to significant dependence of N_o upon the viscoelastic properties. Consequently, the theory will not be valid during those periods for which such inhomogeneities exist.

A study of the possible ways in which the fracture properties may change is beyond the scope of this paper. But we will comment briefly on temperature dependence of the creep compliance as a large amount of experimental data exists on this property. For many crystalline and amorphous polymers, below and above the glass-transition temperature, T_g, temperature dependence of the compliance is characterized under isothermal conditions by the simple equation [1],

$$C_v(t, T) = C_o + \Delta C(\xi)/a_G \tag{101}$$

where

$C_o = C_o(T)$ = initial compliance

$\Delta C(\xi) \equiv (C_v - C_o)\, a_G$

$\xi \equiv t/a_T$ = reduced time

$a_G = a_G(T)$ = compliance factor

$a_T \equiv a_T(T)$ = time-scale factor

Thus, three functions of temperature (C_o, a_G, a_T) plus one function of reduced-time ($\Delta D(\xi)$) define the compliance $C_v(t, T)$. It should be added that most of the data used to establish the form of Eq. (101) are from uniaxial tensile tests; however, this equation should be quite accurate for C_v as well since the uniaxial creep compliance and C_v differ by only the factor $(1 - \nu^2)$.

Let us assume the common power law form for $\Delta C(\xi)$,

$$\Delta C(\xi) = C_R \xi^m \tag{102a}$$

where C_R and m are constants. Upon comparing Eqs. (96) and (102a) we see that C_2 is a function of temperature; viz.,

$$C_2 = C_R / a_T^m\, a_G \quad . \tag{102b}$$

This coefficient, as well as $C_o(T)$, can be substituted directly into Eq. (97) in order to predict crack growth under different constant or transient temperatures.

When amorphous polymers are in their glass-to-rubber transition

[illegible] one can neglect the temperature dependence of a_G and C_o, and therefore write

$$C_v \equiv C_v(\xi) \tag{103}$$

where $\xi = t/a_T$. Any material whose temperature dependence enters entirely through the time scale, as in Eq. (103), is called "thermorheologically simple"[13].

Prediction of Initial and Intermittent Crack Growth

The preceding analysis enables one to predict crack growth under a constant or varying stress intensity factor during those periods for which N_o, Γ, and σ_f do not vary appreciably over each time increment $\alpha/\dot{a}$. Of course, even if there are intervals during which this condition is not met, the theory is still valid for predicting growth in each intervening period when N_o is sufficiently large.

Prediction of the time at which a crack starts to grow (i.e., the fracture initiation time, t_i) and growth when N_o varies significantly during the time increment $\alpha/\dot{a}$ (as in low stress level fatigue) is accomplished by bringing together the convolution representation of displacement, Eq. (41), the finite stress condition, Eq. (22), and the fracture energy Eq. (54) or Eq. (55). The analysis may be considerably more involved than the preceding one of continuous growth since simplified displacement Eq. (82) cannot be used and the energy Γ and failure stress distribution

will possibly depend on loading history. Because of this complexity we shall limit our analysis to the prediction of t_i and initial velocity using an idealized representation of σ_f. A possible approach to analyzing more general problems will be outlined at the conclusion of this section. Environmental and aging effects are omitted for simplicity.

Fracture Initiation Time: Suppose that the crack tip is initially located at x = 0 and that the body is subjected to load(s) starting at t = 0. As the first case we assume (i) N_o is a nondecreasing function of time, and (ii) the failure stress distribution is constant (viz., $\sigma_f \equiv \sigma_m$ = constant). The length of the failure zone is found from Eq. (22),

$$\alpha = \frac{\pi^2 N_o^2}{4\sigma_m^2} \quad . \tag{104}$$

Inasmuch as the left end of the failure zone (see Fig. 1) does not completely fail until an amount of work equal to ΓdA has been done on it, the failure zone length in Eq. (104) is also equal to the movement of the crack tip during the first stage of loading.
The crack opening displacement at the left end (x = 0) is obtained from Eq. (41) by substituting Eq. (42) with x = 0 and $a(\tau) = \alpha(\tau)$, and then using Eq. (104) for α; there results,

$$v = \frac{\pi N_o^2}{4\sigma_m} C_v^{(2)} \tag{105}$$

where $C_v^{(2)}$ is a so-called "secant compliance,"

$$C_v^{(2)} = C_v^{(2)}(t) \equiv \frac{1}{N_o^2(t)} \int_o^t C_v(t - \tau) \frac{d\, N_o^2(\tau)}{d\tau} d\tau \quad . \qquad (106)$$

Failure of the material at $x = 0$ occurs when v reaches the value v_m, corresponding to the displacement for which the energy input is equal to Γ; specifically, from Eq. (54),

$$\Gamma = \sigma_m v_m \quad . \qquad (107)$$

Setting $t = t_i$ and $v = v_m$ in Eq. (105) and substituting this result into Eq. (107) we obtain

$$\Gamma = \frac{\pi}{4} N_o^2(t_i)\, C_v^{(2)}(t_i) \qquad (108)$$

which is identical to the condition for the onset of crack growth in an elastic body except the secant compliance, Eq. (106), replaces $4(1 - \nu^2)/E$ (see Eq. (59)). Referring to Eq. (94), we conclude that $t_i = 0^+$ if $N_o(0^+) \geq N_{og}$, and that fracture does not initiate if $N_o < N_{oe}$.

Secant compliance Eq. (106) can be rewritten as follows:

$$C_v^{(2)}(t) = C_v(t) - \frac{1}{N_o^2(t)} \int_o^t [C_v(t) - C_v(t - \tau)] \frac{d\, N_o^2(\tau)}{d\tau} d\tau \qquad (109a)$$

Since N_o and C_v are nondecreasing functions of time, this equation implies

$$C_v^{(2)}(t) \leq C_v(t) \quad . \qquad (109b)$$

Hence, if the creep compliance itself were used in the elastic-like Eq. (108) instead of the secant compliance, the predicted initiation time, t_{ci}, say, would satisfy the condition

$$t_{ci} \leq t_i \quad . \tag{109c}$$

The equality results if N_o is constant for $t > 0$.

When N_o is a power law in time, the secant compliance can be obtained from the previous result for effective compliance, Eq. (79). Namely, if $N_o \sim t^{\mu}$, where μ is a positive constant, we find

$$C_v^{(2)}(t) = \lambda_{nr} C_v(t) \tag{110}$$

where λ_{nr} is given by Eq. (80) and $r = 2\mu$. Figure 6 can be used to estimate λ_{nr} if $1/2 \leq \mu \leq 7/4$.

The fracture initiation time predicted by Eq. (108) was derived assuming $\sigma_f = \sigma_m$ = constant. However, the results in Appendix C provide evidence that Eq. (108) is at least approximately valid even if f varies with ξ. Specifically, when approximate displacement Eq. (49) is used along with Eq. (22) to predict v_m, and it is assumed that the shape of the failure zone is the same as in Eq. (72) (viz., $v \sim \xi^{n+3/2}$) and that $\sigma_f = \sigma_m F(v/v_m)$, there results

$$\Gamma = A_i \frac{\pi}{4} N_o^2(t_i)\, C_v^{(2)}(t_i) \tag{111a}$$

where A_i is given by

$$A_i \equiv -\frac{8}{3} \frac{I_2}{I_1^2} \int_0^1 F(\rho)\, d\rho \quad . \tag{111b}$$

The coefficient A_i turns out to be equal to the ratio Γ_{ap}/Γ in Eqs. (C-4) and (C-5) when σ_f is given by Eqs. (C-1) and C-2), respectively. In view of the results shown in Fig. C-1, it is tentatively concluded that Eq. (108) can be used to predict fracture initiation time even when σ_f varies with ξ. (There are cases, however, when t_i is very sensitive to Γ and therefore very sensitive to the variation of σ_f. For example, this situation exists when N_o is a constant within the range in Eq. (94a) and $C_v^{(2)}$ is a weak function of time.)

Let us now consider the problem of predicting fracture initiation time when we remove the assumption that N_o is nondecreasing but, for simplicity, retain the assumption that $\sigma_f = \sigma_m$. Equation (104) implies the position of the crack tip $a(= \alpha)$ will move to the left ($\dot{a} < 0$) upon unloading ($dN_o/dt < 0$) if σ_m does not decrease at least in proportion to N_o; result $\dot{a} < 0$ is physically unacceptable since it would imply complete healing of the material in the failure zone and, moreover, would invalidate Eq. (41) since it is restricted to $\dot{a} \geq 0$. At any time ($0 < t \leq t_i$) during the loading or unloading periods the displacement is given by Eq. (41) as long as $\dot{a} \geq 0$ and the crack faces do not contact one another (which could occur if $N_o < 0$). At $x = 0$ and with $\sigma_f = \sigma_m(\tau)$ and $\xi = a = \alpha(\tau)$, we find

$$v = \frac{1}{\pi} \int_0^t C_v(t - \tau) \frac{d}{d\tau} [\sigma_m(\tau)\ \alpha(\tau)]\ d\tau \quad . \tag{112}$$

One physically reasonable selection for $\sigma_m(\tau)$ and $\alpha(\tau)$ would be σ_m = constant when $dN_o/dt > 0$ and $N_o \geq N_o(\max)$, where $N_o(\max)$ is the largest N_o up to the present time, and α = constant whenever $N_o < N_o(\max)$.

The analysis will not be pursued further in this paper. However, it is to be noted that the resultant work input to the failure zone at $t = t_i$ should be calculated using Eq. (55), rather than Eq. (107), since σ_m is time dependent.

Initial Velocity: Calculation of tip velocity during the first stages of crack growth will be illustrated using the assumptions that N_o is nondecreasing and $\sigma_f = \sigma_m$ = constant. Motion of the crack tip prior to t_i is obtained directly from Eq. (104) since $da/dt = d\alpha/dt$:

$$\frac{da}{dt} = \frac{\pi^2 N_o}{2\sigma_m^2} \frac{dN_o}{dt} \qquad 0 < t < t_i \quad . \tag{113}$$

Immediately after fracture initiates, the tip velocity becomes dependent on the creep compliance of the continuum. This velocity can be calculated from Eq. (91) if N_o does not change appreciably during the time it takes for the crack to propagate the distance α in Eq. (104). Inasmuch as N_o satisfies Eq. (108) at t_i, comparison of Eqs. (91) and (108) yields an implicit equation for $\dot{a}$,

$$C_v(\lambda_n^{1/n}\, \alpha/\dot{a}) = C_v^{(2)}(t_i) \tag{114}$$

where $t_i < t < t_i + \alpha/\dot{a}$. If, for example, N_o is constant for $t > 0$ and $N_{oe} < N_o < N_{og}$,

$$C_v^{(2)}(t_i) = C_v(t_i) \tag{115a}$$

and therefore,

$$\frac{\alpha}{\dot{a}} = t_i/\lambda_n^{1/n} \tag{115b}$$

or

$$\dot{a} = \frac{\lambda_n^{1/n}}{t_i} \cdot \frac{\pi^2 N_o^2(t_i)}{4\sigma_m^2} \tag{115c}$$

which is the velocity immediately after the fracture initiates at time t_i. Referring to Fig. 6, it is seen that $0.29 \leq \lambda_n^{1/n} \leq 0.40$ when $0 \leq n \leq 1$; thus, according to Eq. (115b) the time for the crack to propagate the distance α is approximately three-times the initiation time. In deriving Eq. (115b) it was assumed that the value of n obtained from the creep compliance at $t = \alpha/3\dot{a}$ (see Eq. (92c)) is the same as that at t_i; this is justified since Eq. (115b) and the average value of $\lambda_n^{1/n} \sim 1/3$ imply $\alpha/3\dot{a} \approx t_i$.

Equation (114) is based on the assumption that the fracture energy required to produce the initial failure at $x = 0$ is equal to that under continuous growth. Whether or not this assumption is valid probably depends on the material and loads since the former energy could depend on loading history when $t < t_i$ and the latter energy may be velocity dependent. Furthermore, an element of material in the failure zone at $x = 0$ is unstressed in the x-direction for $t > 0$, while in the continuous growth case an element of material in the failure zone is under triaxial stress at least part of the time.

Low Stress Level Fatigue: When Eq. (91) cannot be used to predict tip velocity, we must return to the convolution

representation of displacement, Eq. (41), in order to establish a criterion for crack growth. Such may be the case in the important problem of cyclic loading when the maximum stress intensity factor is large enough to cause crack growth while the minimum factor is so low that either the crack is stationary during a portion of each cycle or $\alpha/\dot{a}$ is not small compared to the vibration period.

The method of analysis used by Knauss and Dietmann [7] apparently could be applied to the present theory; they expanded the stress intensity factor in a power series in time over the interval in which the crack moved a distance α, where α was constant in their theory. Here it would be necessary to account as well for the fact that α, and possibly σ_f, vary with time over each cycle, but such an analysis will not be pursued in this paper.

4. Applications

A Sheet Under Constant Stress

Consider a centrally cracked plate, such as shown in Fig. 9. Assuming the crack length, 2a, is large compared to sheet thickness but small compared to the in-plane dimensions, the stress intensity factor is [5],

$$N_o = \sqrt{\frac{a}{2}}\,\sigma \tag{116}$$

where σ is the applied stress. Crack growth and failure time will be predicted using Eq. (97) under the assumption that the creep

compliance parameters, C_2 and m, and the fracture properties, Γ and $\sigma_m I_1$, are constant. Substitution of Eq. (116) into Eq. (97), assuming σ is applied at $t = 0$ and is constant thereafter, and integrating yields

$$t = \frac{2}{\pi^2} \frac{\sigma_m^2 I_1^2}{\sigma^2} \left(\frac{C_o}{\lambda_m C_2}\right)^{1/m} \int_1^{a/a_o} \left[\frac{a_g}{a_o \gamma} - 1\right]^{1/m} \frac{d\gamma}{\gamma} \qquad (117a)$$

where a_g is defined as

$$a_g \equiv \frac{8\Gamma}{\pi C_o \sigma^2} \quad . \qquad (117b)$$

When the central crack reaches length $2a_g$ complete failure of the sheet occurs; this point follows from Eqs. (91), (94c), and (116), which imply $\dot{a} \to \infty$ as $a \to a_g$. The time at which $a = a_g$ is called the <u>failure time</u>, t_f, which, after changing the intergration variable in Eq. (117a), becomes

$$t_f = \frac{2}{\pi^2} \frac{\sigma_m^2 I_1^2}{\sigma^2} \left(\frac{C_o}{\lambda_m C_2}\right)^{1/m} \int_{a_o/a_g}^1 (1 - u)^{1/m} u^{-(1+1/m)} du \quad . \qquad (118)$$

It is of interest to notice that when $a_g/a_o >> 1$ and $0 \leq m \leq 1$, the integrand in Eq. (117a) goes quickly to zero as γ increases. In fact, the current time is already 90% of t_f when

$$\frac{a}{a_o} \simeq 10^m \quad . \qquad (119)$$

One can easily show that if the assumption $a_g/a_o >> 1$ is removed, the crack growth at $t = 0\ 90\ t_f$ will be even less than given in Eq. (119).

These observations are important because they tell us if the stress intensity factor, Eq. (116), is valid over most of the time period $0 \leq t \leq t_f$ or if the effect of finite sheet width must be included when predicting failure time. For three typical values of m, Eq. (119) yields

$$\frac{a}{a_o} \simeq \begin{cases} 10 & , m = 1 \\ 3.3 & , m = 0.5 \\ 1.6 & , m = 0.2 \end{cases} . \tag{120}$$

Surprisingly, most of the time required for failure is consumed while the crack is still relatively small, especially for $0 \leq m \leq 0.5$.

As a point of comparison, if the bracketed term in the integrand in Eq. (117a) is replaced by $(a_g/a_o\gamma)^{1/m}$ for all $0 \leq t \leq t_f$, the failure time is derived by setting $a/a_o = \infty$ to find

$$t_f = \frac{2m\ \sigma_{m\ \perp}^{\angle}}{\pi(2+1/m)} \left(\frac{8\Gamma}{\lambda_m C_2 a_o}\right)^{1/m} \sigma^{-2(1+1/m)} \tag{121}$$

which brings out very simply the effect of stress on failure time. This is the same result as would be obtained by neglecting (N_o^2/N_{og}^2) in Eq. (97) at the outset of the analysis.

Equations (118) and (121) will be compared to experimental data on Solithane 50/50, which is a crosslinked, amorphous, polyurethane rubber. The experimental data, which are shown in Fig. 9, have been normalized with respect to the stress σ_∞, where

$$\sigma_\infty \equiv \sqrt{\frac{8\Gamma E_\infty}{3\pi a_o}} \tag{122}$$

is the critical stress for the onset of crack growth in an elastic plate having Poisson's ratio $\nu = 1/2$ and Young's modulus $E_\infty = 4(1 - \nu^2)/C_v(\infty) = 3/C_v(\infty)$; thus, no crack growth occurs for $\log(\sigma/\sigma_\infty)^2 \leq 0$. Also, all data have been reduced to a common temperature of 0°C by recognizing that the material is essentially thermorheologically simple [5]; according to Eq. (103) the effect of temperature can be introduced by replacing t_f with t_f/a_T in Eq. (118). Since $\log(t/a_T) = \log t - \log a_T$, the theory, if valid, implies experimental failure data obtained at different temperatures can be superposed by means of horizontal translations of magnitude $\log a_T$ so as to form a single curve; the failure data at the temperatures indicated in Fig. 9 were shifted to the data at 0°C. (One can interpret the reduced failure data as being the results of tests conducted entirely at 0°C.) We should add that the creep compliance in Fig. 4 was formed in the same way; in fact, the values of $\log a_T$ used to shift the failure data are those obtained by shifting the creep compliance. That a single creep compliance curve was obtained is a check on the thermorheological simplicity assumption; the fact that the failure data superpose extremely well (as seen in Fig. 9) using the same values of $\log a_T$ helps to substantiate the assumption that Γ and σ_m are constant, and checks the underlying fracture theory itself.

In view of the power law fit shown in Fig. 4, we set $m = 0.5$ in Eq. (118) and carry out the integration to find

$$t_f = \frac{2}{\pi^2} \frac{\sigma_m^2 I_1^2}{\sigma^2} \left(\frac{C_o}{\lambda_m C_2}\right)^2 \left\{\frac{3}{2} + \frac{1}{2}\left(\frac{a_g}{a_o}\right)^2 - 2\frac{a_g}{a_o} + \ln \frac{a_g}{a_o}\right\} \qquad (123)$$

where a_g depends on stress through Eq. (117b). When $a_g/a_o \gtrsim 30$ this equation reduces to Eq. (121) after setting $m = 1/2$. The latter equation shows the theory is a straight line with slope of $-1/3$ when $\log(\sigma/\sigma_\infty)^2$ is plotted against $\log t_f$; it is observed in Fig. 9 that this is indeed the slope of the experimental data in the low stress level range ($(\sigma/\sigma_\infty)^2 \lesssim 10^{0.75}$).

Referring to Eq. (121), we see that the influence of the fracture properties on the relation between σ and t_f in the straight line region is through the combination $(\sigma_m I_1 \Gamma)$. Had the fracture data been given in terms of σ in [5], rather than σ/σ_∞, this combination of properties could have been found by matching the theory and experiment at any point in the straight line range. (Note that $\sigma_m I_1$ and Γ appear by themselves in the high stress level range of Eq. (123); if the theory is applicable in this range one can then determine $\sigma_m I_1$ and Γ separately.) Knauss [5] obtained the fracture energy itself from other experiments on swollen rubber, in which state the material is essentially elastic, and then used the corresponding value of σ_∞ to normalize the failure data. He found $\Gamma = 2.41 \times 10^{-2}$ lb/in., which corresponds to $\sigma_\infty = 8.40$ psi. (Knauss actually reported the value of $\Gamma = 3.21 \times 10^{-2}$ lb/in. [5],

but this value was obtained by using the plane stress equation for critical stress in an elastic sheet; later it will be found that α is much less than sheet thickness, which means the plane strain version should have been used. In order to correct the reported Γ value we have multiplied it by $(1 - \nu^2) = 3/4$. Now, express Eq. (121) in terms of (σ/σ_∞) and solve for $\sigma_m I_1$ by noting that the straight line in Fig. 9 intercepts the stress axis at $t_f = 10^8$ sec $= 10^{6.22}$ min; hence

$$\sigma_m I_1 = 172 \times 10^3 \text{ psi} \quad . \tag{124a}$$

By taking into account Eq. (24b), a lower bound to the maximum failure stress is obtained:

$$\sigma_m \geq 86 \times 10^3 \text{ psi} \tag{124b}$$

where the equality is used if σ_f is constant throughout the failure zone. The ideal theoretical strength based on failure of a regular arrangement of carbon atoms is approximately thirty-times this value [19]; however, considering the irregular nature of real networks, the presence of shear forces at the tip (see Fig. 3) and that Eq. (124b) is the lower bound and not necessarily σ_m, this numerical result does not seem unreasonable.

Inasmuch as both $\sigma_m I_1$ and Γ are now known, we can plot the remainder of the solution as given by Eq. (123). While having the correct shape, the theory underpredicts failure time in the high stress level range above $\log (\sigma/\sigma_\infty)^2 \simeq 0.8$, say; this stress

corresponds to an overall strain of approximately 5%. Since $t_f \sim N_o^{-6}$ for m = 1/2, even a small amount of nonlinearity, such as blunting of the crack tip and consequent reduction of stress intensity factor, could have a significant effect. In fact, we find the theory agrees with all of the experimental results if the stress intensity factor in Eq. (116) is replaced with

$$N_o = (1 + 2\varepsilon)^{-1} \sqrt{\frac{a}{2}}\, \sigma \tag{125}$$

(It is to be noted that the effective modulus of the sheet is a constant 430 psi since the time scale for crack growth in Fig. 9 is far beyond the viscoelastic range in Fig. 4.)

Even though the stress at the tip is very high (Eq. (124b)), the strain is not because practically equal triaxial tension exists. Using a typical value of bulk modulus, 2×10^5 psi, the Young's modulus of 430 psi, $\sigma_x = \sigma_y$, and $\sigma_z = \nu(\sigma_x + \sigma_y)$ we find $\varepsilon_x = \varepsilon_y \simeq 21\%$. Moreover, because $\sigma_y = \sigma_m + 0(\xi_1^{1/2})$ near the tip, the strain decays rapidly along the line of crack prolongation.

The length of the failure zone is found from Eq. (92b). For the lowest and highest stresses at which experimental data are shown in Fig. 9 we find, respectively

$$\text{(i)} \qquad \log(\sigma/\sigma_\infty)^2 = 0.2 : \quad \alpha = \begin{cases} 0.6 \times 10^{-8} \text{ cm}, & t = 0^+ \\ 2.0 \times 10^{-8} \text{ cm}, & t = 0.9\, t_f \end{cases} \tag{126a}$$

$$\text{(ii)} \qquad \log(\sigma/\sigma_\infty)^2 = 1.6 : \quad \alpha = \begin{cases} 10 \times 10^{-8} \text{ cm} , & t = 0^+ \\ 32 \times 10^{-8} \text{ cm} , & t = 0.9\ t_f \end{cases} \tag{126b}$$

where Eq. (125), rather than Eq. (116), has been used to calculate stress intensity factor. Although the accuracy of the theory in predicting failure zone lengths comparable to interatomic spacing (Eq. (126a)) is suspect, it is believed the scale is at least correct in view of the agreement between experiment and theory in the low stress level range; if α were constant, for example, a slope of (-1/2), rather than (-1/3), would be predicted for the graph in Fig. 9. (In an attempt to bracket the actual failure zone size, stationary and moving cracks were observed with the TAMU scanning electron microscope. Figure 11 shows a tip which was moving at approximately 10^{-3} in./min at 77°F. Cracks at 10x the magnification of this figure were also studied visually but the failure zone was still too small to be observed; because of excessive discharging, with and without a coating, the resolution of the crack boundary was not as good as in Fig. 11.)

The instantaneous value of $\alpha/\dot{a}$ is found from Eqs. (92b) and (97) to be a <u>decreasing</u> function of N_o. Therefore, the largest $\alpha/\dot{a}$ for the entire set of experiments occurs at $t = 0^+$ under the lowest stress. We find

$$\frac{\alpha}{\dot{a}}\,(\max) = 14 \times 10^{-2} \text{ min} \quad . \tag{127}$$

Referring to Fig. 4, we see $(\alpha/3\dot{a})(\max)$ is practically within the

range of the generalized power law creep compliance; since $(\alpha/\dot{a}) \sim N_o^{-4}$ and Eq. (127) is based on a_o (rather than a), use of Eq. (96) with m = 1/2 is justified in all predictions of failure times. Moreover, the maximum fracture initiation time is approximately $(\alpha/3\dot{a})(\max)$ and therefore t_i is negligible relative to the range of t_f in Fig. 9.

Additionally, as required by the underlying theory, the change in stress intensity factor over each time increment $\alpha/\dot{a}$ is small for the entire experimental range of behavior; this observation follows from Eq. (127) and the fact that the increase in N_o during most of the propagation time is small according to Eq. (120).

A Long Strip under Constant Strain

The previously determined creep compliance and fracture properties of Solithane 50/50 will be used in conjunction with Eq. (97) to predict constant velocity crack propagation in the long strip shown in Fig. 10. Provided a > 1.5b, the stress intensity factor in a strip clamped to rigid grips is [6],

$$N_o = \left\{\frac{b(1 - \nu^2)}{2\pi}\right\}^{1/2} \sigma \qquad (128)$$

where σ is the stress which must be applied to the clamps to produce the strain ε. Although this applied stress and strain could vary with time, the experimental results are for the case in which the strain is held constant and the strip is in a fully relaxed state outside the neighborhood of the tip; thus $\sigma = E_\omega \varepsilon/(1 - \nu^2)$, which

when substituted into Eq. (128) yields

$$N_o = E_\infty \left(\frac{2b}{3\pi}\right)^{1/2} \varepsilon \qquad (129)$$

where we have set $\nu = 1/2$.

Theoretical upper and lower bounds on strain for which stable growth exists in the Solithane are obtained by using Eq. (94); there results

$$-1.89 < \log \varepsilon < -0.81 \quad . \qquad (130)$$

These bounds are drawn with dashed lines in Fig. 10.

Except at high strains, the predicted velocities are seen to be in very good agreement with the experimental data. (If the stress intensity factor in Eq. (129) is divided by $(1 + 2\varepsilon)$, as in Eq. (125), the predictions at the high strains are likewise found to agree.) Whenever N_o^2/N_{og}^2 can be neglected in the denominator in Eq. (97) we find $\dot{a} \sim \varepsilon^6$, and therefore the theory plots as straight lines in Fig. 10 with slope of 1/6; the upper strain limit for this behavior is found to be at $\log \varepsilon \simeq -1.2$.

It should be pointed out that Mueller and Knauss [6] gave a value of Γ which is three times that reported in Knauss' constant stress study [5] and used above. This larger value cannot be reconciled with the existence of failure data under low values of constant stress in [5], and therefore was not used in any of the calculations made here.

For the range of experimental data in Fig. 10, Eq. (92b) with

N_o corrected for finite strain as mentioned above, yields

$$0.70 \times 10^{-8} < \alpha < 53 \times 10^{-8} \text{ cm} \quad . \tag{131}$$

The largest value of $\alpha/3\dot{a}$, after converting to T = 0°C, is 0.9×10^{-3} min; this result implies, of course, that the generalized power law in Fig. 4 is valid for the entire experimental range.

Variable Loading and Properties; the Linear Cumulative Damage Rule

Some consequences of Eq. (95) concerning crack growth and failure will be examined and then compared with experimental results on two different particulate composites: solid propellant and asphaltic concrete. For reasons of clarity, we first introduce some simplifying assumptions. Although they may not be satisfied exactly in practice, it is believed there are many applications in which the resulting error will have little effect on the total time required for failure.

Except for some later observations, we assume (i) n is constant. The other material properties (C_1, Γ, $\sigma_m I_1$) may be functions of time (which, for example, could be due to a transient temperature and/or aging) but we assume (ii) their variation during most intervals $\alpha/\dot{a}$ is small. Also, motivated by Eq. (115b), we assume (iii) fracture initiation time for the initial loading (as well as for subsequent reloading if there are periods for which $\dot{a} = 0$) is negligible. Finally, it is assumed (iv) that the stress intensity factor depends on only one length parameter defining either the

crack size "a" (say) or local geometry of the body "h" (say). From dimensional considerations,

$$N_o = \sqrt{a}\, L \tag{132}$$

or

$$N_o = \sqrt{h}\, L \tag{133}$$

where "L" is a linear function of the stresses applied to the body; e.g., see Eqs. (116) and (128). The size "a" may represent the radius of an isolated internal (penny-shaped) crack or the half-length of an isolated through-crack. The parameter "h" could be the separation of two rigid boundaries, where the crack length or diameter has to be at least somewhat greater than h; recall that $a > 1.5b$ is sufficient for the plane problem in Fig. 10.

It should be emphasized that if there are periods when the stress intensity factor is negative (due to, for example, cyclic loading having a zero mean value) the analysis is not invalidated. For the above assumptions (ii) and (iii) together with Eq. (95) imply $\dot{a}$ during growth periods depends on the instantaneous stress intensity factor and not on either its history or the stress history. The following equations will be given without explicitly writing $\dot{a} = 0$ whenever $L < 0$; however, one should set $L \equiv 0$ during all periods in which L is actually negative.

Supposing first that Eq. (132) applies, integration of Eq. (95) and setting $a = \infty$ yields an implicit equation for failure time, t_f, in terms of the initial half-length, a_o, and material property and load histories,

$$1 = \frac{1}{n}\left\{\frac{a_o \lambda_n \pi^{(2n+1)}}{4}\right\}^{1/n} \int_o^{t_f} \left[\frac{C_1}{\Gamma}\right]^{1/n} \frac{L^{2(1+1/n)}}{\sigma_m^2 I_1^2}\, dt \quad . \qquad (134)$$

This equation can be expressed in a more recognizable form by introducing a new quantity, t_c, where

$$t_c = t_c(t) \equiv \frac{n \sigma_m^2 I_1^2}{L^{2(1+1/n)}} \left\{\frac{4\Gamma}{a_o \lambda_n \pi^{(2n+1)} C_1}\right\}^{1/n} \quad . \qquad (135)$$

Then Eq. (134) becomes simply

$$1 = \int_o^{t_f} \frac{dt}{t_c(t)} \qquad (136)$$

It is easily demonstrated by means of Eq. (134) that $t_c(t)$ would be the failure time for the body if it had timewise constant applied loads and constant material properties equal to those that exist in the actual variable loading problem at the current time t.

If L and the properties are piecewise constant in time, then Eq. (136) becomes

$$1 = \sum_{j=1}^{N_f} \frac{\Delta t_j}{t_{cj}} \qquad (137)$$

where Δt_j is one of the time periods over which the body has constant applied loads and properties, t_{cj} would be the failure time for the body if it had these timewise constant loads and properties from $t = 0$ to failure, and N_f is the number of steps that are needed to produce failure in the actual variable loading case.

Equations (136) and (137) are two forms of the well-known

linear cumulative damage rule which has been used by engineers to predict failure times of specimens and structures (usually with acceptable accuracy) subjected to varying loads, given experimental data on the failure time t_c for constant loads. This rule, but in a slightly different form, was originally proposed by Palmgren [20] and used by Miner [21] as an empirical method of predicting failure under variable amplitude cyclic loading of metals; it is often called "Miner's Hypothesis" or "Miner's Law."

Another feature of Eq. (134) may be brought out by predicting failure under constant loading rate, $\dot{L}$. For simplicity we assume the mechanical and fracture properties are constant. Substituting $L = \dot{L}\, t$ in Eq. (134), and defining the "critical stress intensity factor" N_{cr} by

$$N_{cr} \equiv \sqrt{a_{ox}}\, \dot{L}\, t_x \tag{138}$$

(which is the stress intensity factor existing at the time of failure, t_x, say, referred to the initial crack size a_{ox}, say) yields

$$N_{cr} = \left\{ (3n + 2)\, a_{ox}^{3/2} \sigma_m^2\, I_1^2\, \dot{L} \left[\frac{4\Gamma}{\lambda_n^{\pi(2n+1)} C_1} \right]^{1/n} \right\}^{n/(3n+2)} . \tag{139}$$

The insensitivity of N_{cr} to loading rate, $\dot{L}$, when $0 \leq n \leq 1$ is especially to be noted.

Now, return to Eq. (95), which is not limited to a stress intensity factor of the form in Eq. (132). Still assuming the fracture properties are constant we may express these properties in terms of t_x, N_{cr}, and a_{ox}; Eq. (95) becomes

$$\frac{da}{dt} = \left(\frac{3n + 2}{a_T}\right)\left(\frac{a_{ox}}{t_x}\right)\left(\frac{N_o}{N_{cr}}\right)^{2(1+1/n)} \quad . \tag{140}$$

This equation enables one to predict crack growth and failure of a structure, given the critical stress intensity factor determined experimentally in a simple specimen having initial crack length $2a_{ox}$ and failing in time t_x. In writing Eq. (140) we have assumed thermorheological simplicity and selected a_T to be unity at the temperature of the experiment used to establish N_{cr}. The value of $a_T = a_T(T)$ shown in Eq. (140) corresponds to the instantaneous temperature of the structure of interest.

If instead of taking a specimen to failure, one simply measures the crack velocity, $\dot{a}_x$, corresponding to an instantaneous stress intensity factor, N_x (which need not be restricted to the forms in Eqs. (132) and (133)), then the crack growth equation (95) becomes

$$\frac{da}{dt} = \frac{\dot{a}_x}{a_T}\left(\frac{N_o}{N_x}\right)^{2(1+1/n)} \quad . \tag{141}$$

An advantage of this experimental method over that leading to Eq. (140) is nonlinear effects can be minimized in the test by measuring velocity early in the growth period. However, Eq. (140) does not require a velocity measurement and, therefore, may be more desirable if nonlinearity is not a problem.

Consider now stress intensity factor Eq. (133), in which h is constant. Let us define failure in this case as the time at which

the crack length reaches some preselected value, a_{mx}, say. Then all of the results Eqs. (134) - (137) apply directly to this case after making the substitution

$$\frac{a_o^{1/n}}{n} \to \frac{h^{1+1/n}}{a_{mx} - a_o} \tag{142}$$

in Eqs. (134) and (135).

The sensitivity of crack velocity, and therefore failure time, to stress intensity factor is clearly revealed by Eqs. (140) and (141). Suppose, for example, Eq. (140) is used to predict failure time of a structure having $n = 0.2$, a constant value of N_o, initial flaw length $a_o = a_{ox}$, and failure is defined to occur when the crack grows to ten times its initial length. Suppose further that the experimental failure time is $t_x = 1$ minute and for the structure $a_T = 1$ and $N_o = N_{cr}/2$. We find the structure fails at $t_f \simeq 10$ days. If, however, $N_o = N_{cr}/4$, then $t_f \simeq 100$ years! Obviously, the ability to predict service life of viscoelastic structures is very much dependent on the accuracy of the stress intensity factors. However, because of the variability of material properties and environmental and loading factors, one can expect considerable scatter in failure times when a large number of structures are involved, which is already a well-known empirical fact.

Before turning to the application of the theory to specific materials, it should be emphasized that the cumulative damage rule is <u>not</u> generally valid in the range for which n is time-dependent. A simple illustration is provided by Eq. (97) using stress intensity

factor Eq. (132). Even with a constant value for m, the presence of N_o^2 in the denominator precludes writing the right-hand side in the form f(a) x g(L), which is necessary if the linear cumulative damage rule is to be derived.

Failure of Solid Propellant: Failure data on several different solid propellants (which consist of a cross-linked rubber matrix filled with approximately 75 vol % hard particles having diameters typically on the order of 10-200 microns) under constant uniaxial stress have been reported by Bills et al. [22,23] to fit the equation

$$\frac{D(\psi)}{D_o} = \left(\frac{\sigma_g}{\sigma_T}\right)^k \tag{143}$$

where

$\sigma_T = \sigma(1 + \varepsilon) \simeq$ true stress

σ = engineering stress (constant during test)

ε = engineering strain at failure

σ_g = engineering failure stress below glass transition temperature

$\psi = t_c/a_T q$

q = constant $\simeq 10^8$

a_T = temperature-dependent time-scale factor

t_c = failure time

$D(\psi)$ = uniaxial propellant creep compliance ($= D_R \psi^n$ in the range of ψ for which the experimental failure data exist, where D_R and n are essentially independent of temperature)

and

$$D_o = D(o) \ .$$

Also, $1.5 \tilde{<} k \tilde{<} 2.5$ is approximately constant for any one propellant. In the referenced work [22], the relaxation modulus, $E(\psi)$, is used instead of $D(\psi)$; to obtain Eq. (143) we have applied the quasi-elastic approximation

$$E(\psi)\ D(\psi) \simeq 1 \tag{144}$$

which is quite good for the usual range of n, $0.15 \tilde{<} n \tilde{<} 0.25$ [24]. It was found that failure did not occur when the tensile stress was below some relatively small value, which evidently corresponds to the stress for which $N_o \tilde{<} N_{oe}$ (see Eq. (94b)). In writing Eq. (143) it is implied that the stress is above this lower limit.

The theoretical equation (135) will be cast in the same form as Eq. (143); in doing this we obtain a partial check on the theory and enable the empirical constants (k,q) to be evaluated in terms of basic material properties. First, note that Eq. (48), together with the fact that $\nu \simeq 1/2$ and that propellants are (approximately) thermorheologically simple,

$$C_v(\xi) = 3\ D(\xi) = 3\ D_R \xi^n = 3\ \frac{D_R}{a_T^n}\ t^n \tag{145}$$

and therefore

$$C_1 = \frac{3\ D_R}{a_T^n} \tag{146}$$

Next, introduce the stress intensity factor for an (internal) penny-shaped crack of radius a [25]

$$N_{op} \equiv \frac{\sqrt{2a}}{\pi}\,\sigma \tag{147}$$

and define the ratio R as

R ≡ actual stress intensity factor of the most rapidly growing crack in specimen/N_{op}

Then substitute $L = R\,N_{op}/\sqrt{a}$ into Eq. (135), assume $\sigma_T \simeq \sigma$ and find that it becomes identical to Eq. (143) if

$$k = 2(1 + n) \tag{148a}$$

and

$$q = \frac{n}{2}\,\sigma_m^2\,I_1^2\,[\sigma_g R]^{-2(1+1/n)}\,\left[\frac{2\,\Gamma\,\pi}{3a_o\lambda_n D_o}\right]^{1/n} \tag{148b}$$

In order to interpret the parameters in Eq. (135) or (148) in terms of the properties of solid propellant and its constituents, it is essential to consider the size of the failure zone relative to the particle sizes and spacing. Figure 12 shows this zone at the tip of a through-crack in a sheet of propellant. It is seen that the zone is large relative to the particles, and consequently the overall or "effective" properties of the composite propellant are the appropriate ones to use in the fracture model; on the other hand, if the failure zone had been entirely within a relatively large volume of matrix material, the matrix mechanical and failure

properties would be the ones to use in the fracture theory. Now, empirical Eq. (143) was established using specimens without cracks except for naturally existing flaws; the fact that the correlation of stress and failure time for all propellants studied is in terms of propellant compliance (rather than that of the matrix) is believed to imply that the crack tip geometry is similar to that seen in Fig. 12, at least during most of the time required for failure. As further evidence of this point, one can usually see very fine surface cracks (with sizes on the order of the largest filler particles) in a specimen under tensile stress; and these cracks grow only a small amount during most of the time required for failure [24]. Since propellant contains a large percentage of much smaller particles, it is tentatively concluded that typically $2a_o \tilde{>} 200$ microns, and that the failure zone is significantly larger than most of the particles; since the compliance of the surrounding continuum is essentially that of the propellant, $n \simeq 0.2$, and consistent with observations we predict from Eq. (120) that gross failure follows shortly after the largest crack has grown approximately 60% in size.

It is to be observed that Eq. (148a) predicts $k = 2.4$ when $n = 0.2$, which is on the high side of the experimentally determined range $1.5 \tilde{<} k \tilde{<} 2.5$. That the reported values of k are not larger is believed to be primarily due to the reduction of the effective stress intensity factor with strain, as suggested previously in the study of Solithane.

As further evidence of the validity of the theory,

Bills et al. [22,23] have applied the linear cumulative damage rule, Eq. (136), together with Eq. (143), to the failure prediction of solid propellant specimens and structures under monotonic and cyclic temperatures and stresses with considerable success.

One final observation concerns a method of predicting fracture initiation in propellant structures that was originally suggested and successfully applied by Swanson [26]; it was motivated by a technique used widely for metals. Essentially the method consists of applying a constant strain rate to a precracked specimen and noting the critical stress intensity factor and time when the specimen breaks. It is then assumed that a crack in a more complex structure will start to propagate when the stress intensity factor reaches the value determined from the laboratory specimens, even though the stress history in the structure may be different. By referring to Eq. (140) or (141) we can see why such a method is successful, at least for some stress histories. Inasmuch as $n \sim 0.2$, the exponent $2(1 + 1/n) \sim 12$, which implies there is very slow crack growth (relative to laboratory specimen time scale and crack size) when $N_o < N_{cr}$, while the velocity is relatively high when $N_o > N_{cr}$. However, one must be aware of the limitations of this method as, for example, structural failure can occur even though the stress intensity factor is always less than N_{cr}; of course, failure time might be very long relative to the experimental time for failure, t_x.

Fatigue Crack Growth in Asphaltic Concrete: As a result of a

large amount of fatigue testing it has been found that the crack growth per cycle, da/dN, can be expressed as the simple power law [27-29],

$$\frac{da}{dN} = B\, N_{om}^{\beta} \tag{149}$$

where B and β are constant under fixed environmental conditions and input wave shape, and N_{om} is the amplitude of an oscillating stress intensity factor. For beams and plates on foundations with sufficiencly high rigidity $\beta = 4$ at 77°F [27,28]. Probably due to strain effects (e.g., crack tip blunting), values of β somewhat less than 4 have been reported for unsupported specimens [27,29]. Also, it has been noted that β tends to increase with decreasing temperature [29].

We shall show that the theoretical fracture model, Eq. (95), is consistent with these findings. First, introduce the function $w = w(t)$ which defines the wave shape of the stress intensity factor,

$$w \equiv \frac{N_o}{N_{om}} \tag{150}$$

where the maximum value of stress intensity factor during a cycle, which is N_{om}, may vary from cycle-to-cycle. We make the reasonable assumption that crack growth per cycle is small, which implies $w(t)$ is essentially equal to the wave shape of the externally applied loading. Now substitute definition Eq. (150) into Eq. (95) and integrate over a cycle having period t_p; writing the crack growth per cycle, Δa, as da/dN we find

$$\frac{da}{dN} = B_t \, N_{om}^{2(1+1/n)} \tag{151}$$

where

$$B_t \equiv \left\{\frac{C_1 \lambda_n \pi^{(2n+1)}}{4}\right\}^{1/n} \int_t^{t+t_p} \frac{w^{2(1+1/n)}}{\Gamma^{1/n} \sigma_m^2 I_1^2} \, dt \quad . \tag{152}$$

Note that Γ and $\sigma_m I_1$ are shown in the integrand as they could be time-dependent, depending on the complexity of the wave shape and whether or not the crack is stationary during part of the cycle; the exponent n and C_1 are assumed constant during each cycle.

Equality of empirical Eq. (149) and theory Eq. (151) requires

$$B = B_t \quad \text{and} \quad \beta = 2(1 + 1/n) \quad . \tag{153}$$

Interpretation of these results turns out to require that we differentiate between a failure zone which is entirely within the bitumen matrix ("micro-zone") and one which encompasses many aggregate particles ("macro-zone"), with the latter situation being analogous to that in Fig. 12 for solid propellant. For a macro-zone the properties in Eq. (152) and the exponent (n) are those of the asphaltic concrete composite; while there may be exceptions, the typical range of the exponent for the composite is $0 \leq n \tilde{<} 0.5$, at least for temperatures not exceeding 100°F, with n decreasing monotonically with decreasing temperature until it is approximately zero at temperatures below the glass transition temperature [e.g., 30,31]. On the basis of the latter observation, we conclude $\beta \tilde{>} 6$ for a

macro-zone.

This value of β is considerably larger than the values ($\beta \lesssim 4$) commonly reported for asphaltic concrete above 40°F. Thus, we must consider the possibility of the failure zone being entirely within the bitumen. Pursuing this question we found from microscope studies at room temperature that the failure zone is not at all like that in Fig. 12. Rather, the bitumen matrix is so weak (it is a non-crosslinked polymer having a much smaller molecular weight than the propellant binder) that the failure zone of a single crack appears to be confined between individual particles instead of being spread out over many. If there is a sufficiently large neighborhood of bitumen around the tip (which is certainly possible if α is comparable to the zone size in solithane, for example) then the value of n and other material properties in B_t, Eq. (152), would be those for the bitumen. Except at temperatures close to and below the glass-transition temperature of the bitumen, the value $n = 1$, which implies from Eq. (153) that $\beta = 4$, is believed to be appropriate. Besides predicting the experimentally observed value of β at small strains, it is to be noted that the creep compliance of the bitumen is given by $D(t) = D_1 t$ except at short times or at low temperatures [32]; in addition, a state of high triaxial stress, which exists at the tip according to the earlier analysis and in the neighborhood of a tip confined between rigid particles, is known to suppress the glass transition temperature of polymers [33] and thereby extend the temperature range for which

$\beta = 4$ is predicted.

Carrying this interpretation somewhat further, let us consider the micro-zone to be a precursor of a macroscopic crack having total length much larger than α and particle spacing. Then since the local amplitude of stress intensity factor, N_{om}, is proportional to the far-field stress amplitude normal to the precursor, σ'_y, say, we may write

$$N_{om} = g_p \sigma'_y \quad . \tag{154}$$

In the simplest situation Eq. (128) implies $g_p = (3b/8\pi)^{1/2}$, where $2b$ is the distance between adjacent particles and we have set $\nu = 1/2$. More generally, g_p can be expected to depend on particle shape and size as well as spacing. Because of the relative rigidity of the aggregate particles compared to the bitumen, dimensional considerations imply g_p is essentially independent of modulus; then assuming $\nu = 1/2$ for the bitumen, the correspondence principle [13] implies Eq. (154) is valid for viscoelastic media. Now, for a sufficiently long crack,

$$\sigma'_y \simeq N'_{om}/\sqrt{\xi_1} \tag{155}$$

where N'_{om} is the stress intensity factor one would calculate for the asphaltic concrete when viewed as a homogeneous continuum, and ξ_1 is at least somewhat larger than the particle spacing in the neighborhood of the crack tip. Substituting Eq. (155) into (154) and the result into Eq. (151), we obtain a result which is formally

identical to original Eq. (151); viz.,

$$\frac{da}{dN} = B'_t (N'_{om})^{2(1+1/n)} \tag{156}$$

where B'_t depends on particle spacing and geometry, in addition to bitumen properties, while N'_{om} is the "effective" stress intensity factor for the composite material. In general, both B'_t and N'_{om} could be functions of the number of cycles N.

While the above description of crack growth in asphaltic concrete represents at best a tentative model and a partial check on the theory, it does bring out the importance of the microstructure (i.e., particles) in the fracture of composite materials. Proper interpretation of experimental results obviously requires that the failure zone size be known relative to microstructural dimensions, and that the possibility of its size changing appreciably with temperature be recognized.

With n constant, and N'_{om} having the form of either Eq. (132) or (133), cumulative damage rules analogous to Eqs. (136) and (137) are easily derived. The only difference in the result is that t is replaced by the number of cycles, N, and t_c by N_c, where N_c is the number of cycles required to fail a specimen under constant amplitude, N'_{om}, and constant B'_t. The rule Eq. (137) then becomes identical to Miner's Hypothesis.

5. Related Theories

As mentioned in the Introduction, the existing theories of crack propagation in viscoelastic media have already been reviewed in Knauss' recent article [2] and, therefore, such an effort will not be repeated here. Rather, we shall simply compare some results of this paper with closely related ones established by others.

The governing equation derived by Knauss [5] for growth of a central crack in a large sheet (see Fig. 9) and one derived by Mueller and Knauss [6] for a cracked strip (see Fig. 10) have the same form as Eq. (91). Namely, the relations are essentially those for an elastic material except creep compliance replaces the elastic compliance. Although there is some difference in certain details it is surprising how similar the results are, considering the fact that the method of derivation is so different in each case.
In [5], the work done by the continuum on the failing material is approximated using the same relation as for an elastic material (viz., 1/2 force x displacement) along with some other analytical approximations at the crack tip. The result is

$$D(\alpha/\dot{a}) = \frac{2\Gamma}{\pi\sigma^2 a} \quad . \tag{157}$$

In contrast, the approach in [6] to predicting crack propagation in a long strip is to let the crack grow in steps. With the crack stationary, the stress in the failure zone is assumed to decay linearly with time until it vanishes; the tip is then instantaneously

advanced a distance α and the stress again decays linearly in time. With $\nu = 1/2$ the governing equation is

$$G(\alpha/\dot{a}) = \frac{3\Gamma}{2b\epsilon^2 E_\infty^2} \tag{158}$$

where G is the difference of two integrals involving the uniaxial creep compliance; for Solithane it is shown in [6] that $G(\alpha/\dot{a}) \approx D(\alpha/3\dot{a})$. Both Eqs. (157) and (158) were derived using a singular stress distribution along with the assumptions of plane stress and a constant value of α. As we have already discussed, when α is much less than sheet thickness (it is for Solithane) plane strain theory should be used, which accounts for one difference between the results in [5,6] and the theory in this paper. Furthermore, α is not really constant; referring to Figs. 9 and 10, for example, with constant α the slopes of the straight portion of the curves are predicted to be (-1/2) and (1/4), as compared to the actual values of (-1/3) and (1/6), respectively. Finally, since $\lambda_n^{1/n} \approx 1/3$ for all $0 \leq n \leq 1$, according to Fig. 6, the theory in this paper, Eqs. (91) and (92a), shows that the use of $D(\alpha/3\dot{a})$ on the left-hand side of Eq. (158) is essentially correct, while the argument $\alpha/\dot{a}$ in Eq. (157) is three-times too large. In later work dealing with rapidly changing stresses, Knauss and Dietmann [7] removed the assumption of plane stress and considered relatively general crack geometries, but the other features in [6] (i.e., stepwise crack propagation, singular stress, and linear decay with time of stresses near the tip) were retained.

Turning to the prediction of fracture initiation time, t_i, Williams [3] used a spherical flaw geometry in order to establish this time. For a constant stress applied at t = 0, he obtained a relation which is very close to an equation for critical stress in an elastic body. Translating Williams' solution to the notation in Eq. (108) for plane strain, we find his result is obtained if $C_v(t_i)$ is replaced by $2C_v(t_i) - C_v(o)$. Thus, the two theories agree qualitatively for $t_i > 0$ and predict the same critical stress intensity factor when $t_i = 0$. Predictions for time-varying stresses do not lend themselves to such a direct comparison. Additionally, when the stress intensity factor is specialized to that for a penny-shaped crack, Eq. (108) predicts the same fracture initiation time as derived by Wnuk and Knauss [4] for a viscoelastic-perfectly plastic solid having a constant yield stress.

6. Concluding Remarks

A simple theory of crack propagation has been developed and successfully applied to three different unfilled and filled polymeric materials under constant and variable loading. Although the continuum was assumed linearly viscoelastic, the nature of the failure zone is quite arbitrary and, therefore, could include material which is highly nonlinear, rate dependent, and even discontinuous. Under mildly restrictive conditions, an equation for fracture initiation time was derived and found to be very similar

to the elasticity relation for critical stress, except a "secant compliance" appears in place of an elastic constant.

Some influence of finite strains on crack velocity was noted for the three materials studied. The general tendency appears to be that the actual crack velocity falls below the linear theory prediction as the strain is increased; it was suggested that an important cause is geometric nonlinearity, in that crack-tip blunting at high strains could reduce the effective stress intensity factor. An ad hoc modification for finite strain effects in Solithane, in which a simple product form was used, brought the theoretical and experimental results together at high strains. As to whether or not one can normally expect to be able to account for geometric and material nonlinearities in the continuum through such a simple modification is not known at this time. A point of encouragement is that the relaxation modulus of many polymers can be expressed as a product function of strain and time [3].

Although only the opening mode has been analyzed in this paper, it seems reasonable to expect the governing equations for fracture initiation time and crack growth in shearing modes to be analogous to those developed here and, therefore, to be similar to equations for critical stress intensity factors in elastic media. Thus, for the skew-symmetric mode [34] ($\tau_{xy} \neq 0$ along plane of crack prolongation) it is conjectured that, in analogy with propagation Eq. (91),

$$C_v(\tilde{t}_\alpha) = \frac{4\Gamma}{\pi N_2^2} \tag{159}$$

where energy Γ is not necessarily equal to that for the opening mode, and the stress intensity factor N_2 is defined in the singular shear stress distribution near the tip, $\tau_{xy} = N_2/\sqrt{\xi_1}$; while for the antiplane mode [34] ($\tau_{zy} \neq 0$ along the plane of crack prolongation),

$$2J(\tilde{t}_\alpha) = \frac{4\Gamma}{\pi N_3^2} \tag{160}$$

where $J(t)$ is the creep compliance in shear and, just as for N_2, N_3 is defined in the singular distribution $\tau_{zy} = N_3/\sqrt{\xi_1}$. Equations for predicting α in these two modes probably are similar to Eq. (92b), but determination of their exact form requires further analysis.

When two or three stress intensity factors exist simultaneously, and it is assumed that the fracture energy is the same as in the opening mode, we add the work input to the failure zone for each mode and find that Eq. (91) is to be replaced by

$$(N_o^2 + N_2^2)\, C_v(\tilde{t}_\alpha) + 2N_3^2\, J(\tilde{t}_\alpha) = \frac{4\Gamma}{\pi} \tag{161}$$

whenever $N_o \geq 0$. The opening mode does not contribute energy if $N_o \leq 0$ since the displacement in the y-direction is then zero; we must therefore set $N_o \equiv 0$ in Eq. (161) unless N_o is positive.

Without further analysis it is not clear what the length of the failure zone should be under combined loading. Nevertheless, by means of the following idealized problem the nature of the interaction can be demonstrated: Assume $N_3 = 0$, $N_o \geq 0$, the failure stress $\sigma_f = \sigma_m$ = constant with the x- stress component negligible, and a maximum principal stress criterion in which σ_m is the same regardless

of the relative magnitudes of N_o and N_2. By analogy with the derivation of Eq. (92b) we deduce

$$\alpha = \frac{\pi^2}{4\sigma_m^2}\left\{\frac{N_o}{2} + [(\frac{N_o}{2})^2 + N_2^2]^{1/2}\right\}^2 \quad . \tag{162}$$

The major problem in generalizing the opening mode theory to include shearing modes is believed to be that of predicting the direction of crack tip motion, as it is very likely that the crack will not extend in its original plane. An example of the complexity of the problem may be seen in Knauss' paper [35], in which a crack was forced to propagate in Solithane in the antiplane shear mode. Crack growth was found to occur by the opening of semi-penny-shaped cracks which straddle the main crack front at an angle of 45 degrees; i.e., the individual planes of crack extension have normals parallel to the direction of maximum principal stress. In the more general case when two or three modes of loading exist together, one can expect the direction of crack motion to depend at least on some average of the maximum principal stress directions over the failure zone. That the propagation direction does not depend solely on the state of stress at the crack tip ($\xi_1 = 0$) may be argued by considering the stresses in rubber, in which case $\nu \simeq 1/2$; since the opening mode stresses at the tip are essentially equal, the direction of propagation when N_2 and/or N_3 are not zero would be relatively insensitive to N_o, which contradicts observed behavior.

Finally, let us briefly consider the problem of opening-mode

adhesive fracture. The critical stress required to cause propagation of an isolated debond between a linear elastic, incompressible ($\nu = 1/2$) continuum and a rigid substrate is identical to that for cohesive fracture of the continuum itself except the adhesive fracture energy Γ_{ad}, say, replaces the cohesive fracture energy [36]. Moreover, it is a simple matter to show that the extended correspondence principle, which was used in the derivation of Eq. (91), is valid as long as the substrate is rigid and the continuum is homogeneous and incompressible. If these restrictions are essentially met, we suggest that Eq. (91) can be used in predicting propagation of the debond crack after Γ is replaced by Γ_{ad}. However, it is anticipated that some modification of Eq. (92b) for failure zone length will be required as both shear and normal stresses act along the interface.

Acknowledgment

The author would like to acknowledge many helpful discussions with colleagues on the fracture behavior of materials. He is especially indebted to Professor M. L. Williams of the University of Utah for encouraging the author to pursue this problem area; to Mr. K. W. Bills, Jr., of Aerojet Solid Propulsion Company for relating his experience on the fracture of solid propellant; to Professor J. S. Ham of Texas A&M University for elucidating molecular aspects of polymer fracture; and to Mr. N. Conrad of Texas A&M University for providing the pictures in Figures 11 and 12.

References

[1] R. A. Schapery, Viscoelastic Behavior and Analysis of Composite Materials, Texas A&M Univ., Rpt. MM 72-3, August 1972 (to appear in Treatise of Composite Materials, Micromechanics Volume, Academic Press, 1973).

[2] W. G. Knauss, The Mechanics of Polymer Fracture, Calif. Inst. of Techn., Rpt. GALCIT SM 72-5, August 1972 (to appear as lead review article in Applied Mechanics Reviews, 1973).

[3] M. L. Williams, Initiation and Growth of Viscoelastic Fracture, Int. J. Fracture Mechanics, 1 (1965) 292-310.

[4] M. P. Wnuk and W. G. Knauss, Delayed Fracture in Viscoelastic-Plastic Solids, Int. J. Solids Structures, 6 (1970) 995-1009.

[5] W. G. Knauss, Delayed Failure--The Griffith Problem for Linearly Viscoelastic Materials, Int. J. Fracture Mechanics, 6 (1970) 7-20.

[6] H. K. Mueller and W. G. Knauss, Crack Propagation in a Linearly Viscoelastic Strip, J. Applied Mechanics, 38 Series E (1971) 483-488.

[7] W. G. Knauss and H. Dietmann, Crack Propagation Under Variable Load Histories in Linearly Viscoelastic Solids, Int. J. Engineering Sciences, 8 (1970) 643-656.

[8] B. V. Kostrov and L. V. Nikitin, Some General Problems of Mechanics of Brittle Fracture, Archiwum Mechaniki Stosowanej, 22, English Version (1970) 749-776.

[9] R. P. Kambour, Mechanism of Fracture in Glassy Polymers, III. Direct Observation of the Craze Ahead of the Propagating Crack in Poly(methyl methocrylate) and Polystyrene, J. Polymer Science, Part A-2, 4 (1966) 349.

[10] J. C. Halpin, Structural Reliability Characterization of Advanced Composites, Proc. Colloq. on Structural Reliability: The impact of advanced materials on engineering design, J. L. Swedlow, T. A. Cruse, and J. C. Halpin, Eds., Dept. Mech. Eng'g., Carnegie-Mellon Univ. (1972) 275-307.

[11] G. I. Barenblatt, The Mathematical Theory of Equilibrium Cracks in Brittle Fracture, IN Advances in Applied Mechanics, Vol. VII, Academic Press (1962) 55-129.

[12] M. L. Williams, On the Stress Distribution at the Base of a Stationary Crack, J. Applied Mechanics, 24 (1957) 109-114.

[13] Y. C. Fung, Foundations of Solid Mechanics, Prentice-Hall, 1965.

[14] G. A. C. Graham, The Correspondence Principle of Linear Viscoelasticity Theory for Mixed Boundary Value Problems Involving Time-Dependent Boundary Regions, Q. Applied Math., 26 (1968) 167-174.

[15] S. Timoshenko and J. N. Goodier, Theory of Elasticity, McGraw-Hill, 2nd Ed., 1951.

[16] J. D. Ferry, Viscoelastic Properties of Polymers, 2nd Ed., Wiley, 1970.

[17] B. Van der Pol and H. Bremmer, Operational Calculus, Cambridge, 1955.

[18] G. I. Barenblatt, V. M. Entov, and R. L. Salganik, Some Problems of the Kinetics of Crack Propagation, IN Inelastic Behavior of Solids, Mat. Sci. Eng. Series, M. F. Kanninen, W. F. Adler, A. R. Rosenfield, and R. I. Jaffee, Eds., McGraw-Hill (1970) 559-585.

[19] M. K. Davis, Electron Paramagnetic Resorance Studies of Molecular Fracture in Oriented Polymers, Ph.D. Dissertation, Texas A&M Univ. (1970).

[20] A. Palmgren, Die Lebensdauer von Kugellagern, Z. Verein Deutscher Ingenieure, 68 (1924) 339-347.

[21] M. A. Miner, Cumulative Damage in Fatigue, J. Applied Mechanics, 67 (1945) A159-A164.

[22] K. W. Bills, Jr., D. M. Campbell, R. D. Steele and J. D. McConnell, Applications of Cumulative Damage in the Preparation of Parametric Grain Design Curves and the Prediction of Grain Failures on Pressurization, Aerojet Solid Propulsion Co., Final Rpt. 1341-26F (Aug. 1970).

[23] K. W. Bills, Jr., D. M. Campbell, R. C. Sampson, and R. D. Steele, Failures in Grains Exposed to Rapid Changes of Environmental Temperatures, Aerojet Solid Propulsion Co., Final Rpt. 1236-81F (Sept. 1969).

[24] K. W. Bills, Jr. (private communication).

[25] G. A. C. Graham, Two Extending Crack Problems in Linear Viscoelasticy Theory, Q. Applied Mathematics, 27 (1969) 497-507.

[26] S. R. Swanson, Crack Propagation in Solid Rocket Propellant Grains Under Ignition Loading, M.S. Thesis, University of Utah (1968).

[27] K. Majidzadeh, E. M. Kauffmann, and C. L. Saraf, Analysis of Fatigue of Paving Mixtures from the Fracture Mechanics Viewpoint, Fatigue of Compacted Bituminous Aggregate Mixtures, ASTM STP 508 (1972) 67-84.

[28] D. V. Ramsamooj, K. Majidzadeh, and E. M. Kauffmann, The Analysis and Design of the Flexibility of Pavements, Proc. Third Int. Conf. on the Structural Design of Asphalt Pavements, 1, U. of Mich., (1972) 692-704.

[29] C. L. Monismith, R. G. Hicks, and Y. M. Salam, Basic Properties of Pavement Components, Federal Hwy. Administration, Office of Research, Rpt. No. FHWA-RD-72-19 (Sept. 1971).

[30] T. Sugawara, Mechanical Response of Bituminous Mixtures under Various Loading Conditions, Proc. Third Int. Conf. on the Structural Design of Asphalt Pavements, 1, U. of Mich. (1972) 343-353.

[31] K. Nair, W. S. Smith, and C. Y. Chang, Applicability of Linear Viscoelastic Characterization for Asphalt Concrete, Ibid. 277-289.

[32] R. N. J. Saal, Asphalt Systems, Composite Materials, L. Holliday, Ed., Elsevier (1966) 453-474.

[33] J. F. Ferry, Viscoelastic Properties of Polymers, 2nd Ed., Wiley, 1970.

[34] G. C. Sih and H. Liebowitz, Mathematical Theories of Brittle Fracture, IN Fracture, II, H. Liebowitz Ed., Academic Press (1968) 67-190.

[35] W. G. Knauss, An Observation of Crack Propagation in Anti-Plane Shear, Int. J. Fracture Mechanics, 6 (1970) 183-187.

[36] M. L. Williams, The Relation of Continuum Mechanics to Adhesive Fracture, J. Adhesion, 4 (1972) 307-332.

[37] J. N. Goodier, Mathematical Theory of Equilibrium Cracks, IN Fracture, II, H. Liebowitz Ed., Academic Press (1968) 1-66.

Appendices

A. Some Order Properties of Displacement and Stress Near the Tip

We first examine the order of the integral ΔI, Eq. (31), when the failure stress-difference is given by

$$\Delta\sigma_f(\xi) = A\ \xi^q \tag{A-1}$$

in the interval $0 \leq \xi \leq \alpha_1$, where $0 < \alpha_1 \leq \alpha$, A and q are non-zero constants, and $0 < q \leq 1/2$; for this range of q Eq. (15) is met but not Eq. (17). The integral in Eq. (31) is rewritten as follows:

$$\int_0^{\alpha} = \int_0^{\alpha_1} + \int_{\alpha_1}^{\alpha} \quad . \tag{A-2}$$

The second integral is readily shown to be of order $\xi^{3/2}$ by expanding the logarithm in a power series in the variable $\sqrt{\xi/\xi'}$ and letting $\xi \to 0$. The first integral is expressed in terms of a new variable of integration, $\gamma = \sqrt{\xi'/\xi}$, and together with Eq. (A-1) it becomes

$$\int_0^{\alpha_1} = 2A\ \xi^{1+q} \int_0^{\sqrt{\alpha_1/\xi}} \gamma^{2q} \left\{ 2 - \gamma\ \ln\left|\frac{\gamma + 1}{\gamma - 1}\right| \right\} d\gamma \tag{A-3}$$

Again divide the range of integration into two parts,

$$\int_0^{\alpha_1} = 2A\ \xi^{1+q} \left\{ \int_0^{\gamma_1} + \int_{\gamma_1}^{\sqrt{\alpha_1/\xi}} \right\} \tag{A-4}$$

Since we are interested in the order of Eq. (A-4) as $\xi \to 0$, the upper limit and the constant γ_1 are taken to satisfy the inequality $0 \ll \gamma_1 < \sqrt{\alpha_1/\xi}$; this choice of γ_1, together with the series expansion for $\gamma \gg 1$,

$$\gamma \ln\left|\frac{\gamma + 1}{\gamma - 1}\right| \simeq 2 + \frac{2}{3\gamma^2} + \frac{2}{5\gamma^4} + \cdots \tag{A-5}$$

renders Eq. (A-4) as

$$\int_o^{\alpha_1} = 2A\, \xi^{1+q} \left\{B + \frac{2}{3(1 - 2q)} \left(\frac{\xi}{\alpha_1}\right)^{\frac{1}{2} - q} + \frac{2}{5(3 - 2q)} \left(\frac{\xi}{\alpha_1}\right)^{\frac{3}{2} - q} + \cdots\right\} \tag{A-6}$$

where $q \neq \frac{1}{2}$ and B is non-zero and is independent of ξ. When $q = \frac{1}{2}$,

$$\int_o^{\alpha_1} = 2A\, \xi^{1+q} \left\{B + \frac{1}{3} \ln \frac{\xi}{\alpha_1} + \cdots\right\} \tag{A-7}$$

Equations (A-6) and (A-7) together with Eq. (A-2) imply that

$$\Delta I = O(\xi^{1+q}) \tag{A-8}$$

when $0 < q < \frac{1}{2}$ and

$$\Delta I = O(\xi^{3/2} \ln \xi) \tag{A-9}$$

when $q = \frac{1}{2}$. It therefore follows from Eqs. (27) and (30) that the

order of v is also given by Eqs. (A-8) and (A-9) for $0 < q < \frac{1}{2}$ and $q = \frac{1}{2}$, respectively. Note that if $q \to 0$, the displacement $v \to O(\xi)$ which implies the crack cross-section approaches a straight-sided wedge very close to the tip.

The limiting case $q = 0$ corresponds to a constant stress over $0 \leq \xi \leq \alpha_1$; in order that σ_f be continuous to the left at $\xi = 0$, in accordance with Eq. (15), we must take $A = 0$. For this case $v = O(\xi^{3/2})$.

Prediction of the behavior of the stresses near the tip is accomplished in a similar manner. First, we record the resultant stresses, Eq. (19b), after substituting Eq. (28) for σ_f:

$$\sigma_x = \sigma_y = \sigma_f(0) + \sigma_f(0)\left[\frac{2}{\pi}\tan^{-1}\sqrt{\frac{\alpha}{\xi_1}} - 1\right]$$

$$+ \frac{1}{\pi}\sqrt{\xi_1}\int_0^{\alpha} \frac{\Delta\sigma_f(\xi)}{\sqrt{\xi}(\xi + \xi_1)}\, d\xi \qquad \text{(A-10)}$$

where $\xi_1 \geq 0$.

The second term is of order $\xi_1^{1/2}$, which follows from a power series expansion of the arctangent in the variable $\sqrt{\xi_1/\alpha}$. Given the power law, Eq. (A-1), the order of the integral in the third term is established by following essentially the same steps used to analyze ΔI (i.e., Eqs. (A-2) - (A-7)). We find

$$\frac{1}{\pi}\sqrt{\xi_1}\int_0^{\alpha}\frac{\Delta\sigma_f(\xi)}{\sqrt{\xi}(\xi+\xi_1)}\,d\xi = \begin{cases}\frac{A}{\pi}B_\sigma\,\xi_1^q + O(\xi_1^{1/2}) : 0 < q < \frac{1}{2}\\ \\ -\frac{A}{\pi}\xi_1^{1/2}\ln\xi_1 + O(\xi_1^{1/2}) : q = \frac{1}{2}\end{cases} \tag{A-11}$$

where B_σ is non-zero and is independent of ξ_1. Thus,

$$\sigma_x = \sigma_y = \sigma_f(0) + O(\xi_1^q) \tag{A-12}$$

when $0 < q < \frac{1}{2}$ and

$$\sigma_x = \sigma_y = \sigma_f(0) + O(\xi_1^{1/2}\ln\xi_1) \tag{A-13}$$

when $q = \frac{1}{2}$. Note that Eqs. (A-12), (A-13), and (19a) predict these stresses to have a vertical tangent at $\xi_1 = 0$; it can be shown that only for the unlikely situation in which $\sigma_f(\xi)$ has a horizontal tangent at $\xi = 0$ and the integral I_2, Eq. (39), vanishes will the stresses $\sigma_x(\xi_1)$ and $\sigma_y(\xi_1)$ also have a horizontal tangent at ξ_1.

The above order properties for stress and displacement are different from those in [37] because $d\sigma_f/d\xi$ was assumed to be bounded in [37].

B. Criterion for Crack Growth when $\sigma_m \to \infty$

At the outset the normalized failure stress distribution, $f \equiv \sigma_f/\sigma_m$, is assumed to satisfy only the following physically-based assumptions:

(i) $f(\xi)$ is piecewise continuous and non-negative

(ii) $\lim_{\xi \to 0^+} f(\xi) = f(0) > 0$

Now, let us show that α vanishes. To this end, write Eq. (22) in the form

$$\sqrt{\alpha}\, I_1 = \frac{\pi N_o}{\sigma_m} \quad . \tag{B-1}$$

Supposing that the stress intensity factor is finite, we obtain

$$\sqrt{\alpha}\, I_1 \to 0 \quad \text{as} \quad \sigma_m \to \infty \quad .$$

Moreover, the integral I_1, Eq. (23), cannot vanish on account of the above two conditions on $f(\xi)$; hence, $\alpha \to 0$ as $\sigma_m \to \infty$. Letting $\alpha \to 0$ in Eq. (23) yields $I_1 = 2\, f(0)$ and, in turn, Eq. (B-1) yields

$$\lim_{\sigma_m \to \infty} [2\sqrt{\alpha}\, \sigma_m\, f(0)/\pi] = N_o \quad . \tag{B-2}$$

With continuous crack growth, $da/dt > 0$, the total time needed for the crack to propagate the distance α, viz., $t_2 - t_1$, approaches zero. Therefore, assuming $f(0)$, σ_m, and N_o are continuous functions of time, or else are independent of time, Eq. (B-2) shows that α is essentially independent of time during the period $t_1 \leq t \leq t_2$.

In view of these results, we will evaluate the displacement, Eq. (41), and then the fracture energy, Eq. (57), for the case of a very small, constant α. First, write displacement Eq. (41) by making an integration-by-parts and the following change of variables:

$$\eta = \frac{\xi}{\alpha} \quad , \quad \eta_1 = \frac{\xi'}{\alpha} \quad , \quad f = \frac{\sigma_f}{\sigma_m} \tag{B-3}$$

where $0 \leq (\eta, \eta_1, f) \leq 1$. The result is

$$\frac{2\pi\ v}{\sigma_m\ \alpha} = C_v(0) \int_0^1 f(\alpha\eta_1)\left[2\left(\frac{\eta}{\eta_1}\right)^{1/2} - \ln\left|\frac{\sqrt{\eta_1} + \sqrt{\eta}}{\sqrt{\eta_1} - \sqrt{\eta}}\right|\right] d\eta_1$$

$$+ \int_{t_1}^{t^-} C_v'(t - \tau) \int_0^1 f(\alpha\eta_1)\left[2\left(\frac{\eta}{\eta_1}\right)^{1/2}\right.$$

$$\left. - \ln\left|\frac{\sqrt{\eta_1} + \sqrt{\eta}}{\sqrt{\eta_1} - \sqrt{\eta}}\right|\right] d\eta_1\ d\tau \qquad \text{(B-4)}$$

in which $t_1 < t \leq t_2$,

$$\eta = [a(t) - x]/\alpha \qquad \text{(B-5)}$$

in the first line, and

$$\eta = [a(\tau) - x]/\alpha \qquad \text{(B-6)}$$

in the second and third lines. Also

$$C_v'(t) \equiv d\ C_v/dt \qquad \text{(B-7)}$$

is finite and positive for all $t > 0$ for real materials; it is a simple matter to show that $C_v(t)$ is the creep compliance of a plate of infinite extent in the z-direction (i.e., $\varepsilon_z = 0$) and subjected to a constant stress in the x- or y-direction.

Equation (B-4) yields

$$\lim_{\sigma_m \to \infty} [2\pi\, v/\sigma_m \alpha] = C_v(0)\, f(0)\, [2\sqrt{\eta} - (1 - \eta) \ln \frac{1 + \sqrt{\eta}}{1 - \sqrt{\eta}}] \qquad \text{(B-8)}$$

The second and third lines in Eq. (B-4) vanish on account of the finiteness of C_v' and $\int_o^1$, and the fact that $t \to t_1$ as $\sigma_m \to \infty$; recall that $t_1 < t \leq t_2$ where $(t_2 - t_1) \to 0$ as $\sigma_m \to \infty$ for $da/dt > 0$.

Now, change the variables in fracture energy Eq. (57) using definitions in Eq. (B-3) for η and f:

$$\Gamma = \sigma_m \int_o^1 f(\alpha\eta) \frac{\partial v}{\partial \eta}\, d\eta \,. \qquad \text{(B-9)}$$

Rewrite this equation to read

$$\frac{2\pi\, \Gamma}{\sigma_m^2\, \alpha} = \int_o^1 f(\alpha\eta) \frac{\partial}{\partial \eta} [\frac{2\pi\, v}{\sigma_m\, \alpha}]\, d\eta \qquad \text{(B-10)}$$

and let $\sigma_m \to \infty$ (which implies $\alpha \to 0^+$):

$$\lim_{\sigma_m \to \infty} [2\pi\, \Gamma/\sigma_m^2\, \alpha] = f(0) \int_o^1 \frac{\partial}{\partial \eta} \left\{ \lim_{\sigma_m \to \infty} [\frac{2\pi\, v}{\sigma_m\, \alpha}] \right\} d\eta \,. \qquad \text{(B-11)}$$

The process of taking the limit under the integral and inside the derivative is valid on account of the piecewise continuity of $f(\xi)$ for $0 \leq \xi \leq \alpha$ and the boundedness and continuity of the derivative in Eq. (B-10) with respect to $0 \leq \eta \leq 1$ and $\alpha \to 0^+$. Integrate Eq. (B-11) and then use Eq. (B-8) to find

$$\lim_{\sigma_m \to \infty} [2\pi \Gamma/\sigma_m^2 \alpha] = 2C_v(0) f^2(0) \quad . \tag{B-12}$$

The quantity $\sqrt{\alpha}\, \sigma_m f(0)$ can be eliminated between Eqs. (B-2) and (B-12) to obtain the equation for critical stress intensity factor of a brittle elastic solid,

$$N_o = \sqrt{\frac{4\Gamma}{\pi C_v(0)}} \quad . \tag{B-13}$$

The initial value theorem for Laplace transforms [17] may be used in conjunction with Eq. (45) to find

$$C_v(0) = \frac{4[1 - \nu^2(0)]}{E(0)} \tag{B-14}$$

which when substituted into Eq. (B-13) yields Eq. (59).

Graham [25] used a global energy criterion and the singular stress distribution for a large centrally-cracked sheet and for a large body with a penny-shaped crack. He obtained results for the critical stress which are identical to those obtained from Eq. (B-13) when N_o is specialized to these two geometries.

C. Work Input to Failure Zone for a One-Term Representation of v

Work input based on approximate displacement Eq. (72a) will be derived and compared with energy Eq. (91). The following two classes of failure stress σ_f are assumed:

$$\text{(i)} \qquad \sigma_f = \begin{cases} \sigma_m \left[1 - \left(\frac{v}{v_m}\right)^a\right] & ; \ 0 \leq v \leq v_m \\ 0 & ; \ v > v_m \end{cases} \tag{C-1}$$

$$\text{(ii)} \qquad \sigma_f = \begin{cases} \sigma_m & ; \ 0 \leq v \leq v_b \\ \sigma_m \left(\frac{v}{v_b}\right)^{-b} & ; \ v > v_b \end{cases} \tag{C-2}$$

where the quantities σ_m, v_m, v_b, a, and b, as well as C_1 and n in power law Eq. (66), are assumed to be positive constants; in reality they may depend on tip velocity, but for the problem at hand it is not necessary to show this dependence explicitly.

The second distribution rigorously implies $\alpha = \infty$, and we shall use this limit in evaluating the integrals $\int_o^\alpha$. However, from a practical standpoint, if b is sufficiently large the influence of the stress σ_f outside of some finite distance α_{ef}, say, will be negligible; it is assumed that $\alpha_{ef}/\beta << 1$, where β is the length parameter appearing in Eqs. (2) - (4).

The approximate work input derived using displacement Eq. (72a) and the above failure stresses will be denoted by Γ_{ap}. We ratio the results to Γ as given by Eq. (91),

$$\Gamma = \frac{\pi}{4} C_v(\tilde{t}_\alpha) \, N_o^2 \tag{C-3}$$

and obtain, finally:

$$\text{(i)} \qquad \frac{\Gamma_{ap}}{\Gamma} = \frac{2}{3} \frac{\left[a(n + \frac{3}{2}) + \frac{1}{2}\right]^2}{(a + 1)(n + \frac{3}{2})\left[a(n + \frac{3}{2}) - \frac{1}{2}\right]} \qquad \text{(C-4)}$$

where $a(n + \frac{3}{2}) > \frac{1}{2}$, and

$$\text{(ii)} \qquad \frac{\Gamma_{ap}}{\Gamma} = \frac{2}{3} \frac{\left[b(n + \frac{3}{2}) - \frac{1}{2}\right]^2}{(n + \frac{3}{2})(b - 1)\left[b(n + \frac{3}{2}) + \frac{1}{2}\right]} \qquad \text{(C-5)}$$

where $b > 1$. These ratios are plotted in Fig. C-1 for a few different values of the constants. The ratio for the case $a = 1/2$ is rather large at $n = 0$ because this exponent is close to the value ($a = 1/3$) for which the integral I_2, Eq. (39), diverges. We see that for most of the predictions the error is no greater than 33%.

FIGURES

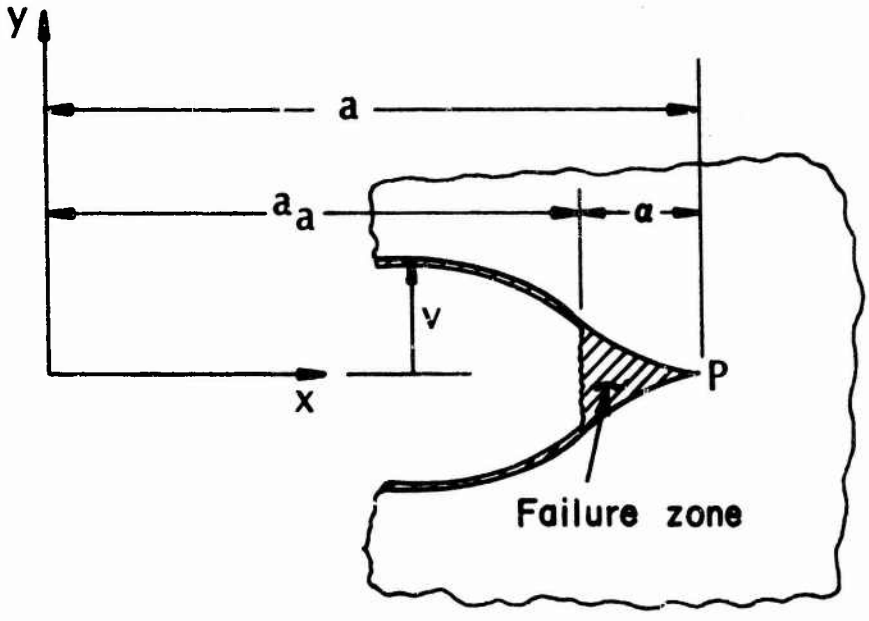

Figure 1. Cross-Section of an Idealized Crack

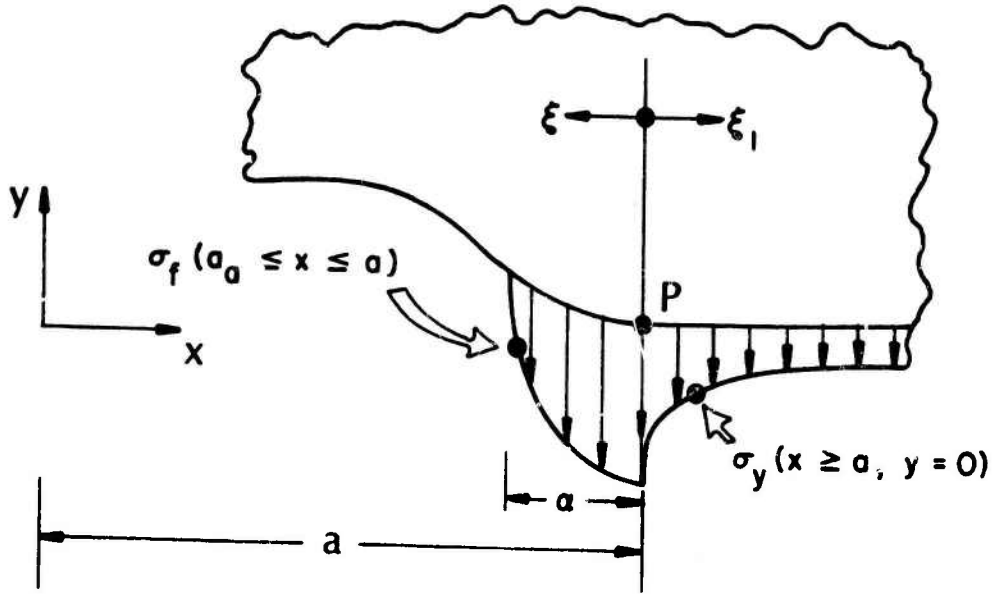

Figure 2. Normal Stress Along Crack Plane

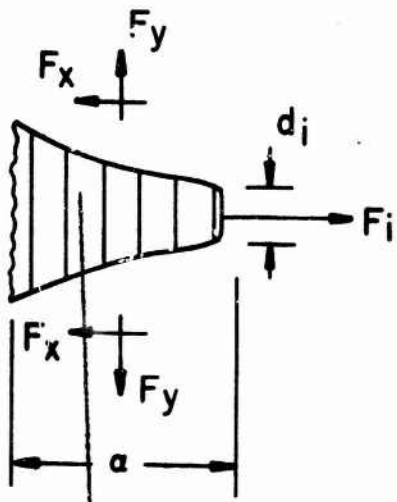

Figure 3. Expanded View of Failure Zone

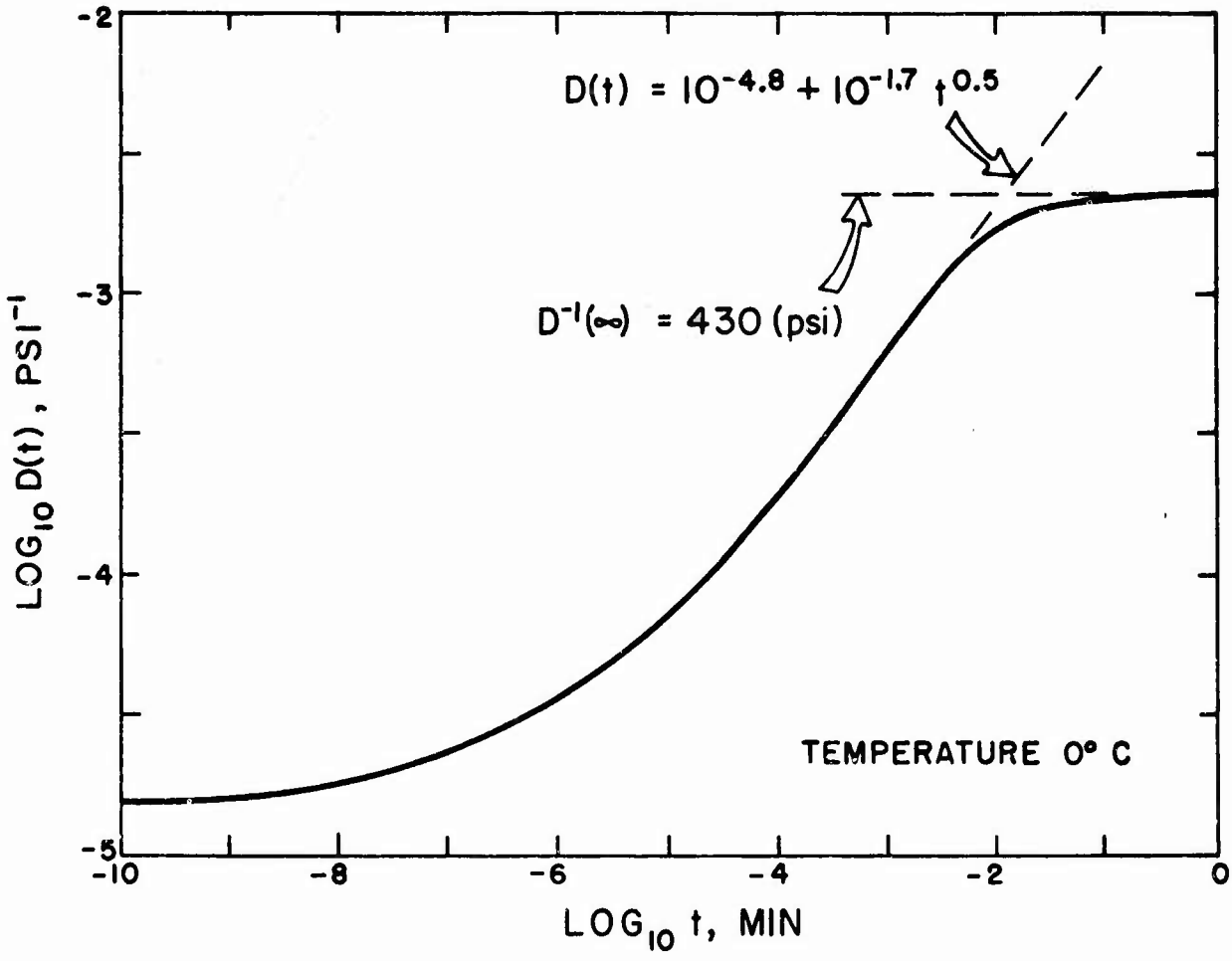

Figure 4. Creep Compliance in Uniaxial Tension for Solithane 50/50 (experimental data, ——, after Mueller and Knauss [6])

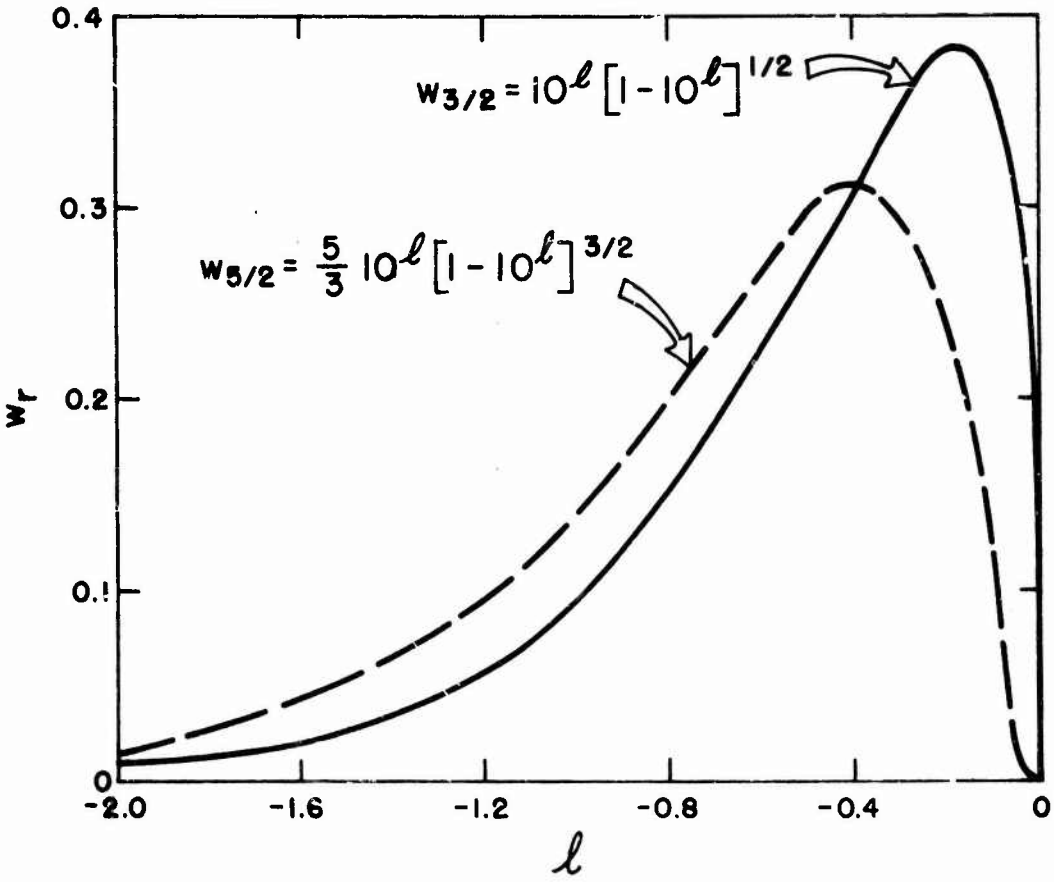

Figure 5. Weighting Functions in the Effective Compliance Integrals

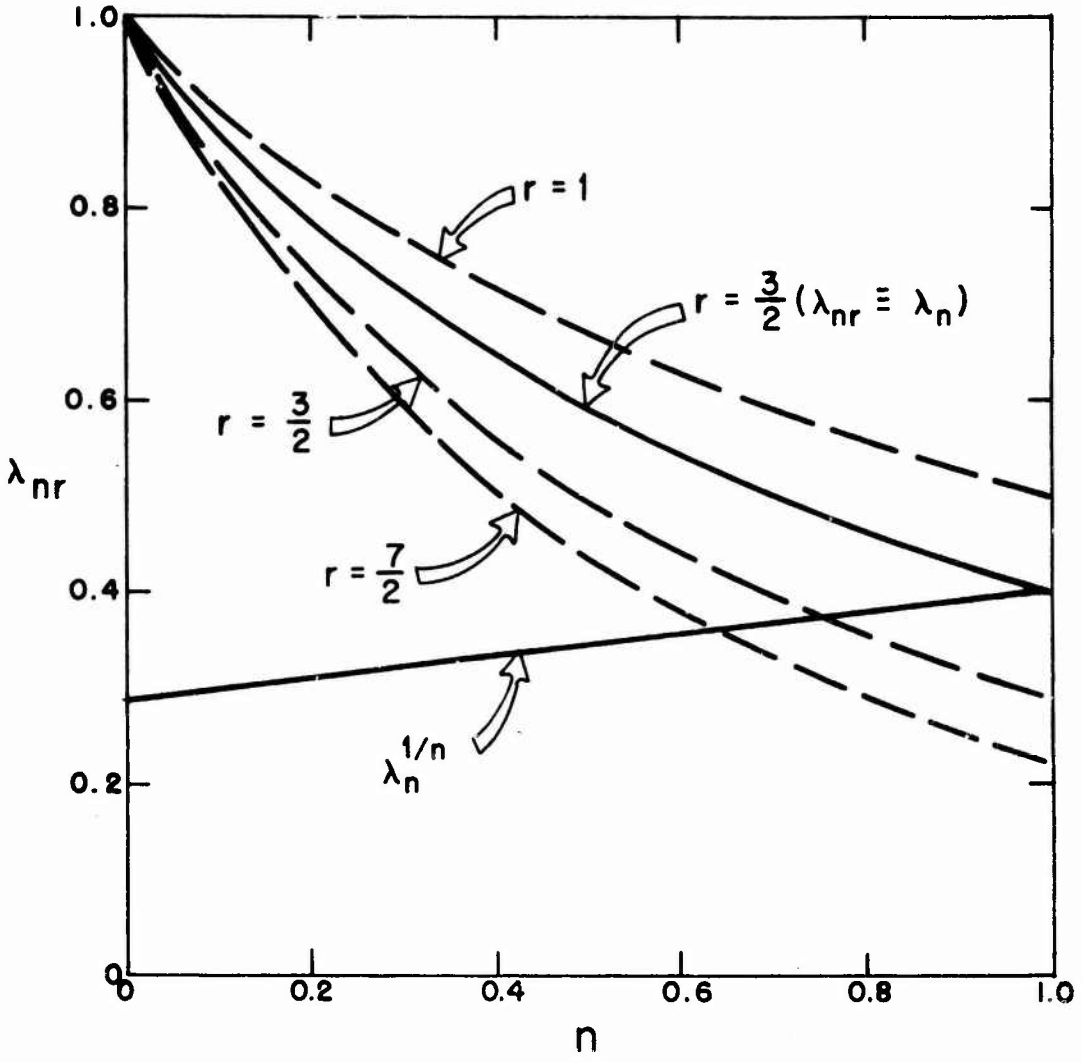

Figure 6. Compliance Coefficient vs. Log-Log Slope of Creep Compliance

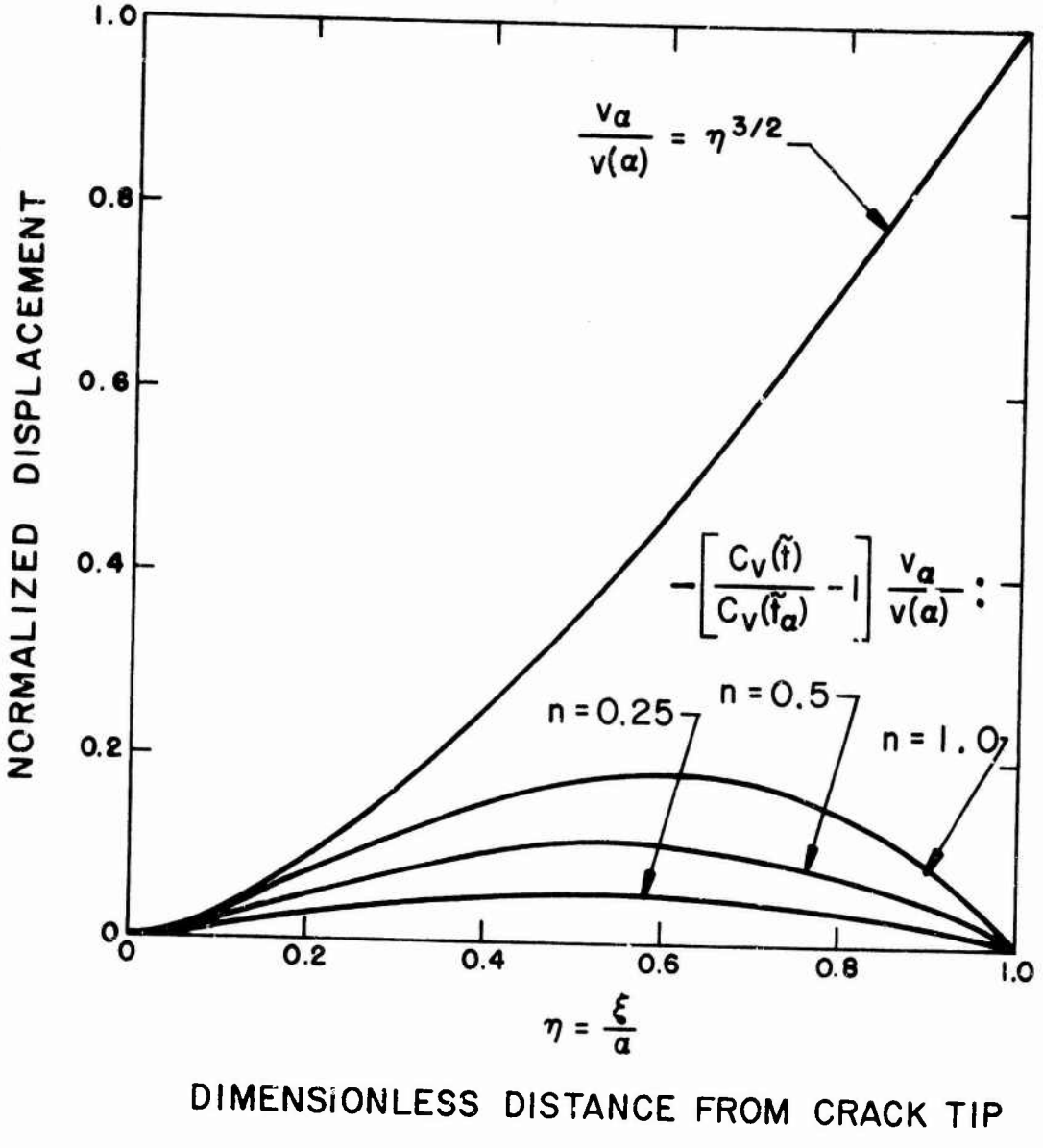

Figure 7. Normalized Displacement Used in Energy Integrals Γ_a and Γ_b

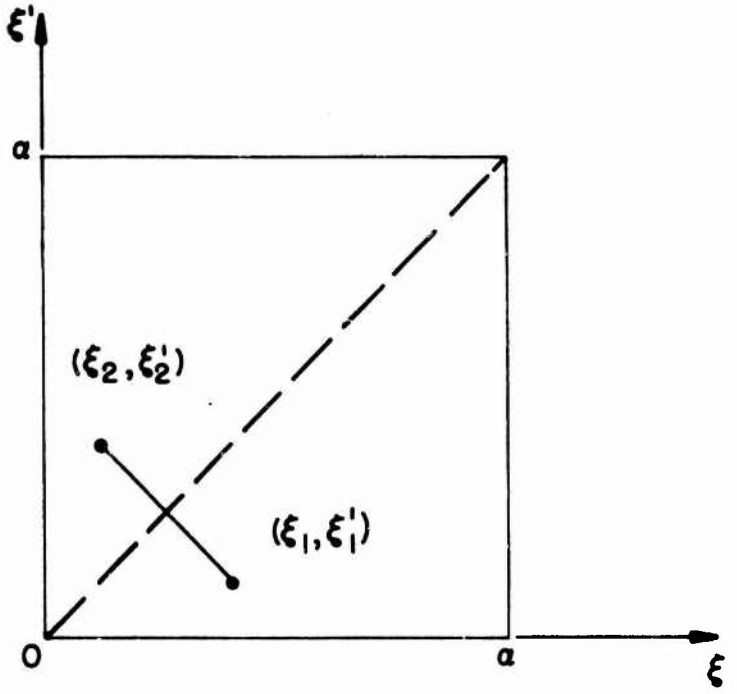

Figure 8. Region of Integration for Integral Z

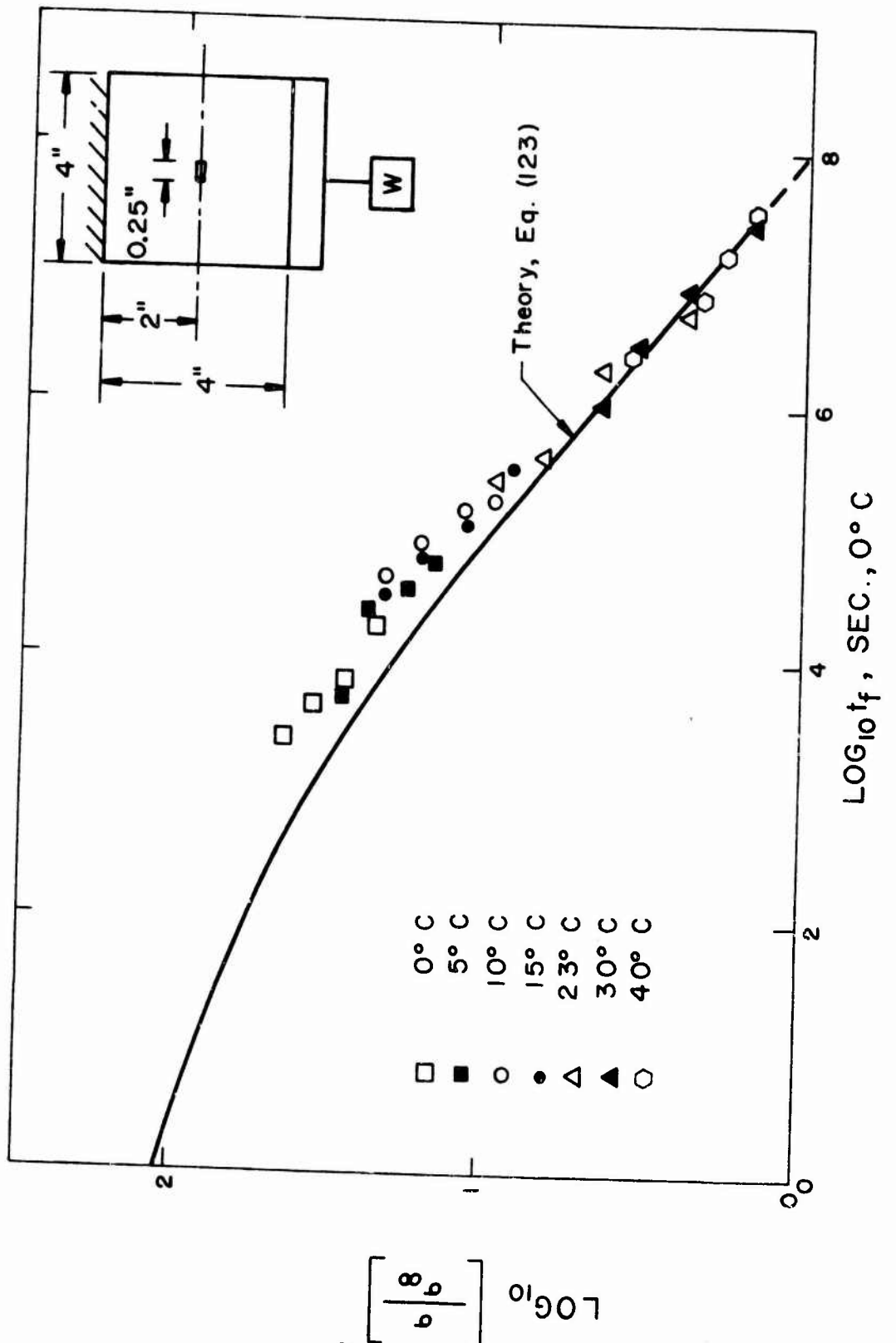

Figure 9. Experimental and Theoretical Failure Times t_f as a Function of the Applied Gross Stress σ for Sollthane 50/50 (experimental data after Knauss [5])

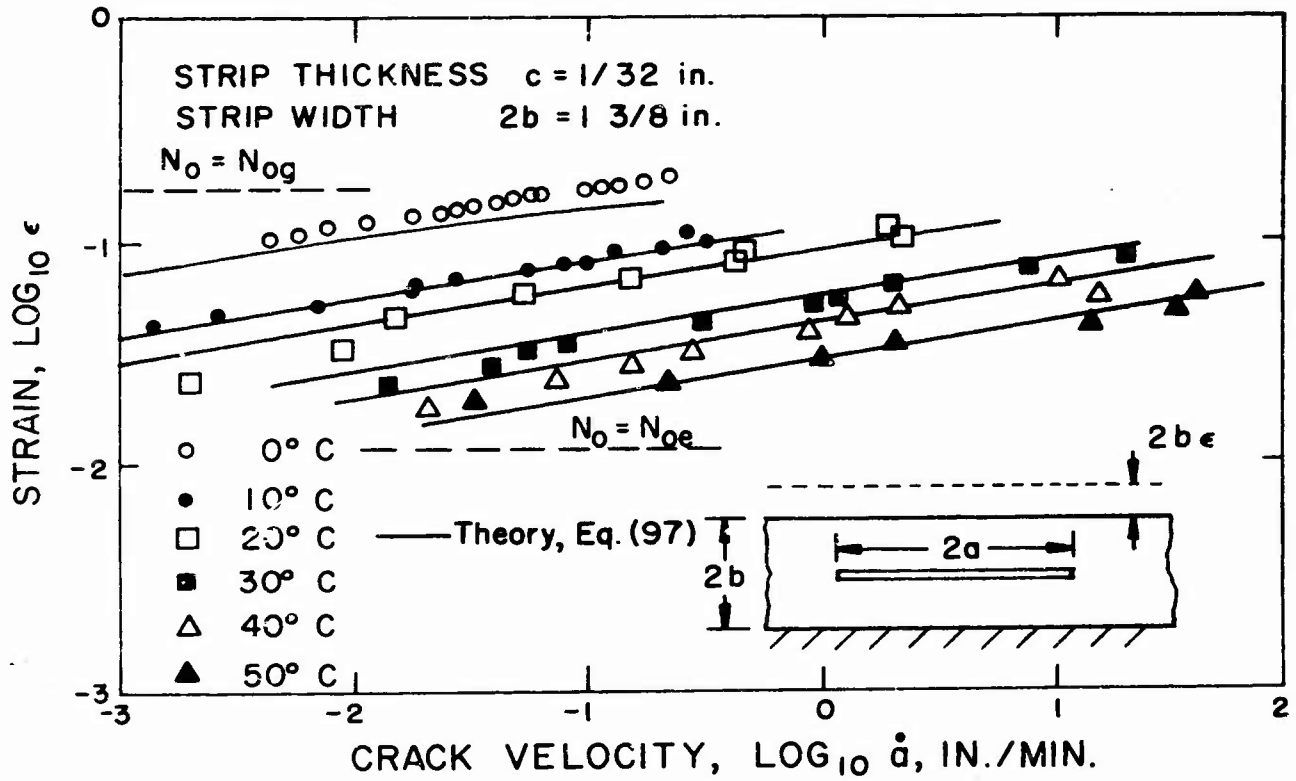

Figure 10. Experimental and Theoretical Crack Velocity as a Function of the Applied Gross Strain ε for Solithane 50/50 (experimental data after Mueller and Knauss [6])

Figure 11. Crack in Solithane 50/50.

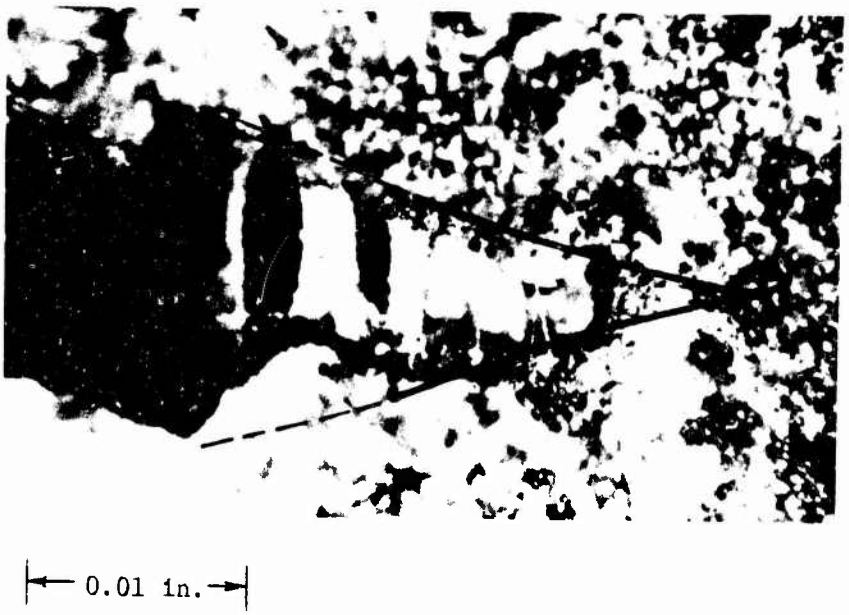

Figure 12. Crack in Solid Propellant.

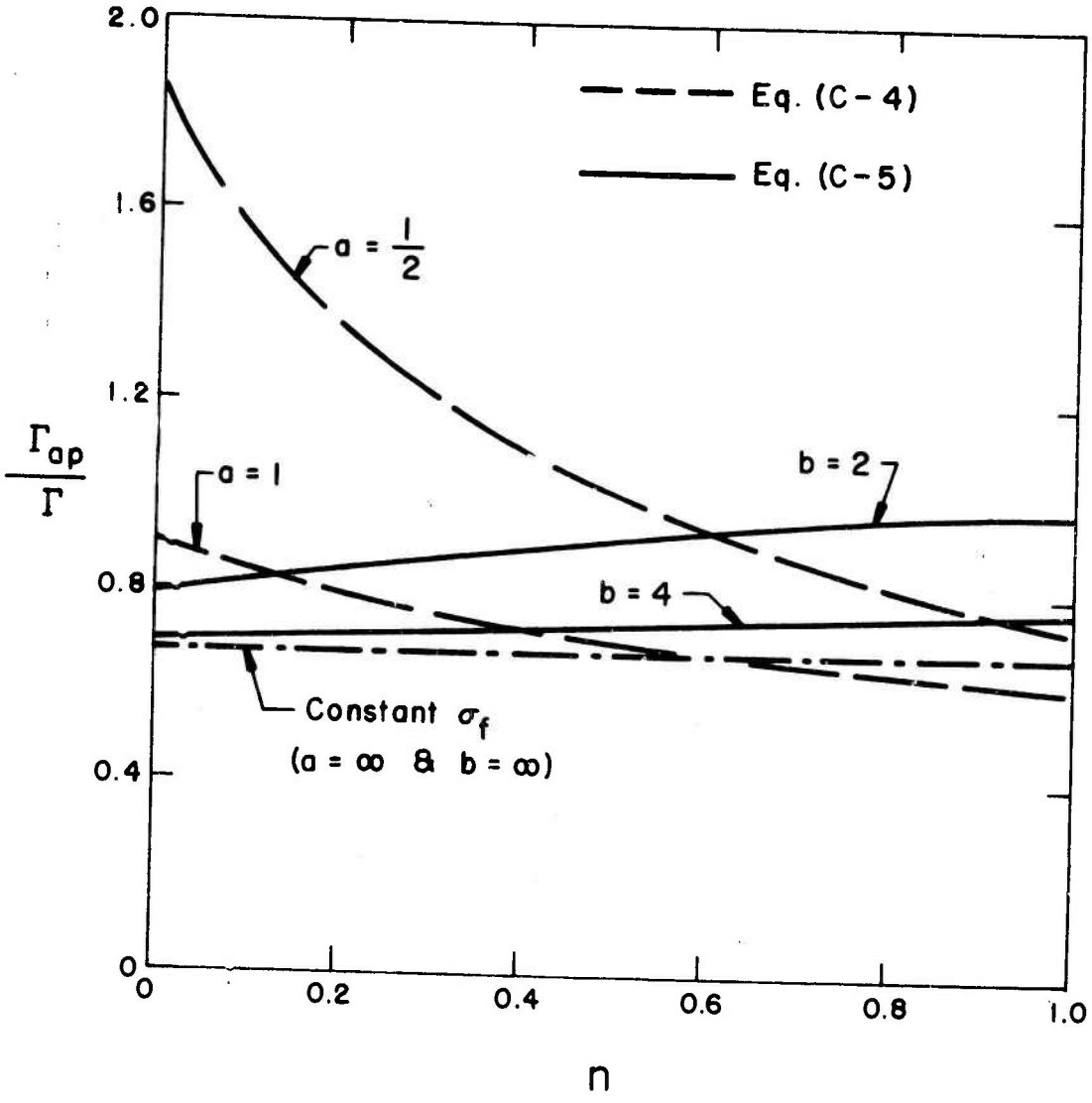

Figure C-1. Ratio of Energies In Failure Zone